# ABSTRACT

## Sulfonated Poly(ether ether ketone)/ETS-10 Pore-filled Poly(tetrafluoroethylene) Nanocomposite Membrane for Improved Ion Selectivity in Vanadium Redox Flow Battery

Lee Yong Kyu

Department of Materials Science and Engineering

The Graduate School

Seoul National University

Titanosilicate ETS-10 has a 3D ordered microporous structure which needs two minus charge of extra-framework cations. Optimum pore size of ETS-10 and unique pore properties are useful for ion selective permeation and proton conduction through micropore.

First, nanocomposite membranes of sulfonated poly(ether ether ketone) (SPEEK) and microporous titanosilicate ETS-10 are prepared with various contents by solution casting to confirm the effect of

titanosilicate as an additive for vanadium redox flow battery applications. The field-emission scanning electron microscopy (FE-SEM) and energy-dispersive X-ray spectroscopy (EDS) images of the composite membrane showed the presence and the uniformity dispersion of ETS-10 in the SPEEK polymer matrix. The water uptake, ion exchange capacity, mechanical property, proton conductivity, vanadium ion permeability and VRB single cell tests of the composite membranes were characterized in detail. The proton conductivity of composite membranes with 1 wt% and 4 wt% ETS-10 loading is improved compared to neat SPEEK membrane. The vanadium permeability decrease as ETS-10 loading due to blocking effect of particles. The composite membrane with 4 wt% ETS-10 which have the highest ion selectivity showed the VRB single cell performance of coulombic efficiency (CE) 99%, voltage efficiency (VE) 80.0% and energy efficiency (EE) 79.2% at 80 mA $cm^{-2}$ resulting from low vanadium permeability without proton conductivity loss. At same cell test condition, Nafion 117 membrane showed the cell performance of CE 98.8%, VE 72.4% and EE 71.4%. Furthermore, the composite membrane with 4 wt% ETS-10 exhibited high capacity retention and maintained efficiency during 100 cycles at 40 mA $cm^{-2}$. The results

indicated that ETS-10 particle is suitable as a permselective barrier for reducing vanadium crossover and improving cell performance.

Second, to improve cycle performances of vanadium redox flow battery, PTFE-based SPEEK/ETS-10 nanocomposite membranes were prepared with various contents by pore-filling method. And same analysis were performed and characterized in detail. The thickness of pore-filled membranes are less than composite membrane series (70 μm and 120 μm respectively). The pore-filled membrane with 3 wt% ETS-10 showed the VRB single cell performance of CE 99.1%, VE 81.6% and EE 81.3% at 80 mA $cm^{-2}$ which slightly higher than the best among composite membrane. Furthermore, the pore-filled membranes showed high capacity retention and maintained efficiency compared to Nafion 117 during 100 cycles at 40 mA $cm^{-2}$. These results indicated that PTFE pore-filling method is effective for improving cyclability and cell performance.


## Keywords

Poly(ether ether ketone), Titanosilicate, Composite membrane, Vanadium redox flow battery, Pore-filled membrane.



***Student number:*** **2014-21460**

# CONTENTS

## 1. Introduction

Due to the environmental pollution and the energy shortages, renewable energy such as solar and wind energy has attracted in recent years [1, 2]. However, the renewable energy is generated intermittently, there is mismatch between power generation and demand [3]. To solve this problem, a safe and effective large scale energy storage system (ESS) is required. Vanadium redox flow batteries (VRBs), developed by Skyllas-Kazacos et al. [4], are estimated as the most suitable candidate ESS for these applications because of their long lifespan, flexible design, high efficiency and fast response time [5-7].

Ion exchange membranes (IEMs) are a key component of VRB systems. IEMs are employed to separate positive and negative electrolytes to prevent them from cross-mixing and allow ion transport to complete the current circuit [8, 9]. An ideal IEM should possess high conductivity, low vanadium permeability, excellent stability, mechanical strength and low cost [10-12]. The membranes most commonly used in VRBs are Nafion, which offer high conductivity and good chemical stability under strongly acidic conditions. However, Nafion membranes have several drawbacks, such as high degree of

vanadium crossover during cell operation causing a reduction of capacity and efficiency of VRB system [13, 14]. In this regard, sulfonated aromatic membranes such as sulfonated poly(ether ether ketone) (SPEEK), sulfonated poly(aryl ether sulfone ketone) and sulfonated poly(sulfone) have been widely investigated as alternative materials [15-19]. Among them, the sulfonated poly(ether ether ketone) is estimated as the most attractive candidate due to its lower vanadium permeability and cost compared to other non-fluorinated membranes.

The properties of SPEEK vary with the degree of sulfonation (DS). It is essential to introduce the functional group (sulfonic acid group) on PEEK for ion exchange. During the sulfonation reaction of PEEK, the more sulfonation proceeds, the higher proton conductivity and ion exchange capacity. However, the reaction induces the poor mechanical property, low chemical stability and the high vanadium permeability, which is detrimental for VRB performance [16, 20].

One approach can be taken to solve this problem is to incorporate inorganic particles into SPEEK matrix such as silicon oxide [21], titanium oxide [22], zeolite [23-25]. This method leads to not only a reduction of vanadium ion crossover by blocking the hydrophilic cluster and introducing the tortuous pathway but also improvement of

mechanical property [15, 26]. Most of inorganic-organic composite membrane shows higher coulombic efficiency due to lower vanadium permeability. However, loading of inorganic particle leads to proton conductivity loss.

The concept of using zeolite materials as an additive for ion exchange polymer has been widely used for DMFC applications [27-30]. By introducing the zeolite particles, methanol permeability can be effectively reduced due to the more tortuous paths and steric hindrance effect for methanol, while proton conductivity loss can be minimized because hydrophilic zeolitic pores and polymer/zeolite boundary act as an additional path of proton. In case of VRBs, vanadium ions are bonded with surrounding water molecules to form hydration shells, while proton exist as polyatomic $H_3O^+$ ions in aqueous solutions without definable hydration cell. Therefore, to pass the zeolitic pores is much hindered for vanadium ion due to the large size. Thus, addition of zeolite also can be effective method for higher ion selectivity for VRBs. However, using zeolite as an additive for VRBs is restrained because the zeolite particles used for DMFC applications were unstable in acidic electrolyte of VRBs. To date, few acid-resistant zeolite-Nafion composite membranes have been studied for VRB applications. In

addition to, these researches focused on minimizing the proton conductivity loss by selective permeation through conventional zeolite pore. Therefore, follow-up study with various combinations of microporous material/polymer composite membranes which can bring further improvement of membrane such as proton conductivity is needed for VRBs applications.

In the present work, we sought to improve the performance of SPEEK for VRBs by introducing microporous Engelhard titanosilicate-10 (ETS-10) particles as an inorganic material. ETS represents a new class of microporous zeolite-type titanosilicate materials, including ETS-4 and ETS-10. These have frameworks that are composed of corner-sharing $SiO_4$ tetrahedra and $TiO_6$ octahedra, resulting in new structures that cannot be built by connecting only tetrahedral units, the only framework units of zeolite [31-33]. The tetrahedral and octahedral are orderly arrayed and forming a 12-membered ring channel with a cross section 7.6 Å × 4.9 Å. Because of the +4 oxidation state of the titanium, every Ti octahedra in the framework needs the two minus charge to maintain electroneutrality, while extra-framework cations of other zeolites are required to balance the one minus charge [34]. In the hydrated state, the extra-framework cations are solvated by water

molecules promoting proton ($H^+$) transport through negative vacancies ($O^{2-}$) by Grotthuss mechanism [35]. Thus, it can contribute to improve the proton conductivity that contributes to voltage efficiency of VRBs. Moreover, sub-micron pore size of ETS-10 can effectively reduce the vanadium ion permeation.

In this work, titanosilicate ETS-10 were synthesized by various condition containing temperature, titanium source, silica source and optimal ETS-10 particle was selected based on the results of X-ray diffraction peak and SEM images. The SPEEK/ETS-10 composite membranes with various ETS-10 contents were prepared by solution casting method. The morphology, physicochemical property, $VO^{2+}$ permeability, mechanical property, and VRB single cell performance of the composite membranes were investigated and discussed in detail. The result obtained for these composite membranes were compared with those of pristine SPEEK and Nafion membranes.

Furthermore, to supplement poor chemical stability and cycle performance of SPEEK/ETS-10 composite membrane, pore-filling method was selected. Pore-filling method is used for reducing swelling ratio and degradation of ion exchangeable polymer [36]. Pore-filling SPEEK/ETS-10 membranes were prepared by pouring SPEEK/ETS-10

composite solution into a porous PTFE membrane and solution casting. Above analysis were performed including VRB single cell performance of the pore-filled membranes. The result obtained for these pore-filled membranes were compared with above SPEEK/ETS-10 composite membranes and Nafion membranes.

## 2. Experimental Section

### 2.1. Materials

Poly(ether ether ketone) (PEEK) (Victrex PEEK 450P) was pretreated by washing and dried at 100 °C. Nafion 117 membranes was purchased from DuPont company. P25 (Degussa, 76% anatase and 24% rutile), $TiO_2$ (Sigma-Aldrich), NaOH (Daejung), NaCl (Daejung), KF (Daejung), Colloidal silica (Sigma-Aldrich, 40% silica), Sodium silicate solution (Sigma-Aldrich), *N*,*N*-dimethylformamide (DMF) (Sigma-Aldrich), HCl (Sigma-Aldrich), $H_2SO_4$ (Sigma-Aldrich), $MgSO_4$ (Daejung), $VOSO_4 \cdot nH_2O$ (Alfa-aesar). All chemicals were used as received.

### 2.2. Synthesis of ETS-10 crystals

ETS-10 was synthesized by using the hydrothermal reaction. Mixture A was prepared by dissolving silica source, NaOH in deionized water for 2 hours. Silica source is sodium silicate solution or colloidal silica. Mixture B was prepared by dissolving a titanium source, namely either P25 (76% anatase and 24% rutile) or titanium dioxide (100% anatase) in deionized water under stirring for 2 hours. The two

mixture were combined by dropwise manner and stirring for 3 hours, resulting in white gel mixture. After aging for 1 day, the mixture was transferred into a Teflon-lined autoclave and placed in an oven at either 200 or 230 ℃ for 2 days. The product was isolated by centrifugation and washed several times with deionized water. The obtained product was dried at room temperature for at least 24 hours. See Fig 1.

### 2.3. SPEEK/ETS-10 composite membrane preparation

Dried 20g of PEEK was dissolved into 200 mL of $H_2SO_4$ (95-98 wt%) with vigorous mechanical stirring at room temperature for 120 hours. The polymer was poured into ice-cold water for precipitation. The polymer was washed with distilled water several times until pH 6-7 and then, dried at 80 °C for 48 hours. The degree of sulfonation of prepared SPEEK was 67% as determined by NMR spectroscopy.

The SPEEK/ETS-10 nanocomposite membranes were prepared by conventional solution casting method as following procedures. First, 1g SPEEK was dissolved in 6mL DMF and filtering by hydrophilic syringe filter to remove impurity. Afterwards, certain amount of ETS-10 was dispersed in 4 mL DMF under sonication for 2 hours. ETS-10 suspension was poured into the polymer solution and resultant mixture

was sonicated for 1h and stirred for 24 hours. The mixture was cast onto a glass dish. The membranes were heated at 60 °C for 4 hours, and then 60 °C under vacuum oven for 24 hours to remove solvents. After solution casting, the membranes were peeled off by pouring water and soaked in 1 M $H_2SO_4$ solution for 24 hours. To clarify effect of ETS-10 particle on membrane properties and VRB performance, nanocomposite membranes with various contents of 0, 1, 4, 7, 10 wt% were prepared. The membranes were termed as S/E*X*, where *X* is the ETS-10 mass ratio. For comparison, a SPEEK blank membrane was prepared under the same condition. See Fig 2.

### 2.4. SPEEK/ETS-10 pore-filled PTFE membrane preparation

The PTFE-based pore-filled SPEEK/ETS-10 membranes were prepared by pouring the composite solution into PTFE membrane and solution casting as following procedures. First, 0.5 g SPEEK was dissolved in 6 mL DMF and filtering by hydrophilic syringe filter to remove impurity. Afterwards, certain amount of ETS-10 was dispersed in 4 mL DMF under sonication for 2 hours. ETS-10 suspension was added to polymer solution and stirring for 24 hours. The mixture was poured into PTFE membrane on glass dish. After shaking smoothly for

impregnation and dispersion of the mixture, the membranes were heated at 60 °C for 24 hours, and then 60 °C under vacuum oven for 24 hours to remove solvents. Post-treatment of the membranes is same above. To clarify effect of ETS-10 particle and pore-filled method on membrane properties and VRB performance, the pore-filled membranes with various contents of ETS-10 were fabricated. The membranes were termed as S/E*X*@P, where *X* is the ETS-10 mass ratio. See Fig 3.

### 2.5. Characterization of synthesized ETS-10 particle

#### 2.5.1. Crystallinity of ETS-10

X-ray diffraction (XRD) was applied to identify the crystallinity of ETS-10, using a New D8-Advanced X-ray diffractometer with $CuK_{\alpha}$ radiation ($\lambda$ = 1.5406 Å) generated at a voltage of 40 kV and a current of 40 mA. The diffraction angle was scanned at a 2° $min^{-1}$ from 10 to 40°.

### 2.5.2. Morphology of ETS-10

Field-emission scanning electron microscopy (FE-SEM) was applied to observe the morphology of the ETS-10 particles and to measure their particle size.

## 2.6. Characterization of membrane

### 2.6.1. Membrane morphology

The morphology of composite membrane cross-section was observed by field-emission scanning electron microscope (FE-SEM). To show the cross-section of membrane obviously, the membranes were located and fractured in liquid nitrogen.

### 2.6.2. Physicochemical property

To evaluate the water uptake and swelling ratio of the membranes, the samples of membrane were soaked in deionized water at room temperature. The membranes were wiped using absorbent paper and measured immediately. Afterwards, the membranes were dried in vacuum oven at 80 °C for 24h. The water uptake of the membranes was defined as weight ratio of the weight changes to that of the dry membranes. It was determined according to the following equation:

$$\text{Water uptake}(\%) = \frac{W_w - W_d}{W_d} \times 100\%$$

Where $W_w$ and $W_d$ are the weight of membrane after and before water absorption, respectively. The swelling ratio was described as the linear expansion rate of wet membrane. It was determined according to the following equations:

$$\text{Swelling ratio}(\%) = \frac{L_w - L_d}{L_d} \times 100\%$$

Where $L_w$ and $L_d$ are the length of membrane after and before water absorption, respectively.

The ion-exchange capacity (IEC) indicates the number of milliequivalents of ions in one gram of the dry polymer. $H^+$ samples were soaked in 50 mL of a 0.05 N NaCl solution for 24 hour at room temperature in order to achieve a complete $H^+$ to $Na^+$ ion exchange. Afterwards, 10 mL of ion-exchanged solution was extracted and titrated with a 0.05 N NaOH solution using phenolphthalein as indicator. IEC was calculated according to the following equation:

$$\text{IEC}(\text{mequiv.}\, g^{-1}) = \frac{V_{NaOH} \times N_{NaOH} \times 5}{W_{dry}}$$

Where $V_{NaOH}$is the volume of consumed NaOH solution and $C_{NaOH}$ is the concentration of NaOH solution.

### 2.6.3. Mechanical strength

The mechanical strength of the membranes was measured by universal test machine at room temperature with a strain rate of 2 mm per minute. The samples were cut into dumbbell shapes with a width of 3.5 mm in the narrow region by press machine. For each test, four measurements were taken and average value was calculated.

### 2.6.4. Proton conductivity

The proton conductivity measurements were carried out on fully hydrated membrane samples with the cell immersed in deionized water [37]. The resistance of membranes was measured in frequency region 1-$10^5$ Hz with an AC current amplitude of 1 mA by Solarton 1255 electrochemical impedance analyzer with a ZPLOT software. The proton conductivity was calculated by using the following equation:

$$\sigma = \frac{L}{R \times A}$$

Where L is the thickness of the membrane and A is the membrane cross-sectional surface area.

### 2.6.5. Vanadium permeability

The permeability of $VO^{2+}$ was measured by membrane-separated diffusion cell. The membrane was placed between two diffusion half

cell. The feed compartment was filled with 1 M $VOSO_4$ in 2 M $H_2SO_4$, and the permeate compartment contained 1 M $MgSO_4$ in 2 M $H_2SO_4$. The two solutions were continuously magnetically stirred to avoid the concentration polarization. The volume of each compartment was 90 mL, and the effective area of the membrane was 3.14 $cm^2$. 5 mL volumes of permeate compartment were extracted at 30 min interval and analyzed by ICP-AES (Agilent Technologies 735 ICP-OES). The vanadium permeability of the membranes was calculated by following equation:

$$V\frac{dC_t}{dt} = S\frac{P}{L}[C_0 - C_t]$$

Where V is the volume of the solution in both compartment, $C_0, C_t$ is the initial concentration and vanadium concentration in the permeate compartment at time t respectively, S is the effective area of membrane, P is the permeability of vanadium ion, and L is the thickness of the membrane. See Fig 4.

## 2.7. Evaluation of membrane performance

### 2.7.1. VRB single cell test

As shown in Fig 5, the VRB single cell was assembled by sandwiching a membrane between two pieces of air-oxidized carbon felt electrodes (XF-30A, Toyobo Co., Ltd) with a polypropylene frame, and two graphite polar plate (SK507, Morgan Korea Co., Ltd) to avoid the corrosion of the copper plates used as current collectors. The effective area of the membrane was 12 $cm^2$, and the volume of the electrolyte solution was 2.8 mL in each half cell. The $VO^{2+}$ solution was prepared by dissolving $VOSO_4 \cdot 3.5H_2O$ (99.9%, Wako Pure Chemical Industrials, Osaka, Japan) in 2 M $H_2SO_4$ solution. The $V^{3+}$ solution was prepared by the electrochemical reduction of the $VO^{2+}$ solution. 2 M $VO^{2+}$ and $V^{3+}$ in 2 M $H_2SO_4$ solutions were used as the initial positive and negative electrolytes, respectively. The cell was charged and discharged using a battery testing system (Maccor 4000) at room temperature. The upper limit of charge voltage and the lower limit of discharge voltage were 1.6 V and 0.8 V to avoid the corrosion of the carbon felt electrodes and conductive plastic, which corresponds to ~100% and ~0% SOC, respectively.

The cycle life test was carried out at the constant current density of 40 mA $cm^{-2}$ with the same cut-off voltage.

The coulombic efficiency (CE), voltage efficiency (VE) and energy efficiency (EE) of VRB single cell were calculated by following equations:

$$\text{CE}\ (\%) = \frac{\int_0^t I_d dt}{\int_0^t I_c dt} \times 100\%$$

$$\text{EE}\ (\%) = \frac{\int_0^t V_d I_d dt}{\int_0^t V_c I_c dt} \times 100\%$$

$$\text{VE}\ (\%) = \frac{EE}{CE} \times 100\%$$

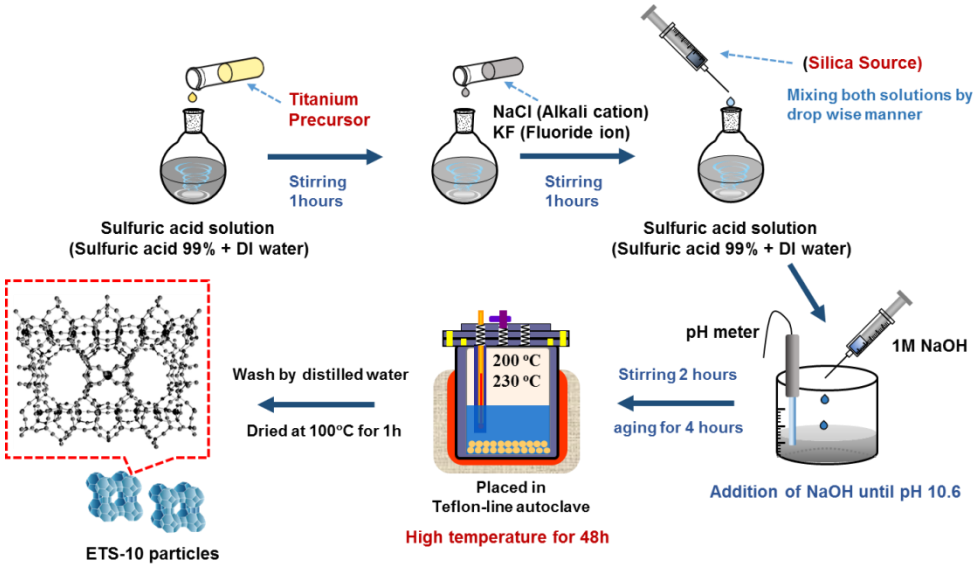


**Fig 1. Synthesis of ETS-10 particle with various conditions.**

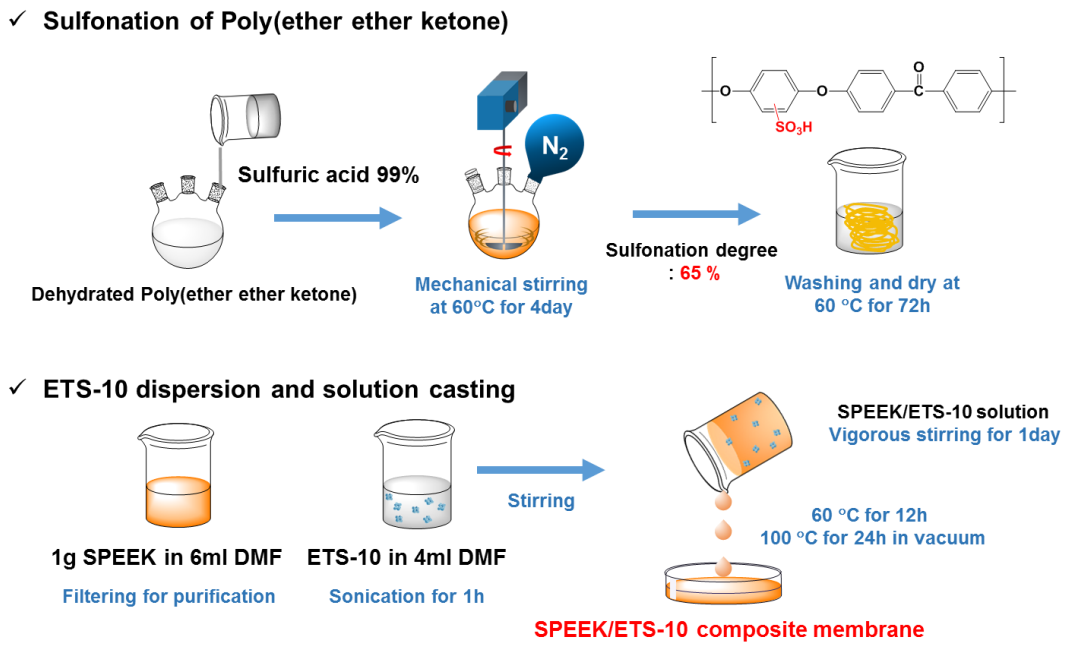


**Fig 2. Sulfonation of poly(ether ether ketone) and preparation of SPEEK/ETS-10 composite membrane.**

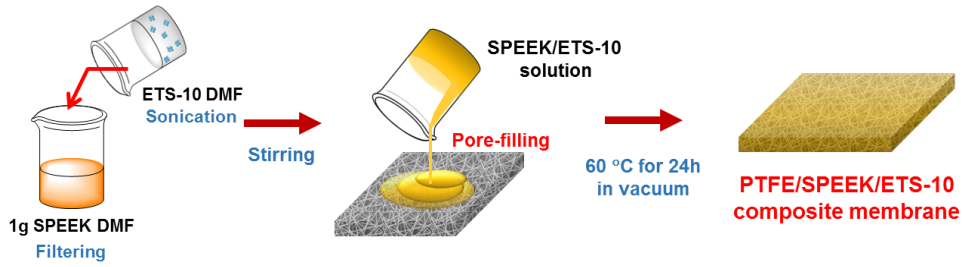


**Fig 3. Preparation of SPEEK/ETS-10@PTFE membrane.**

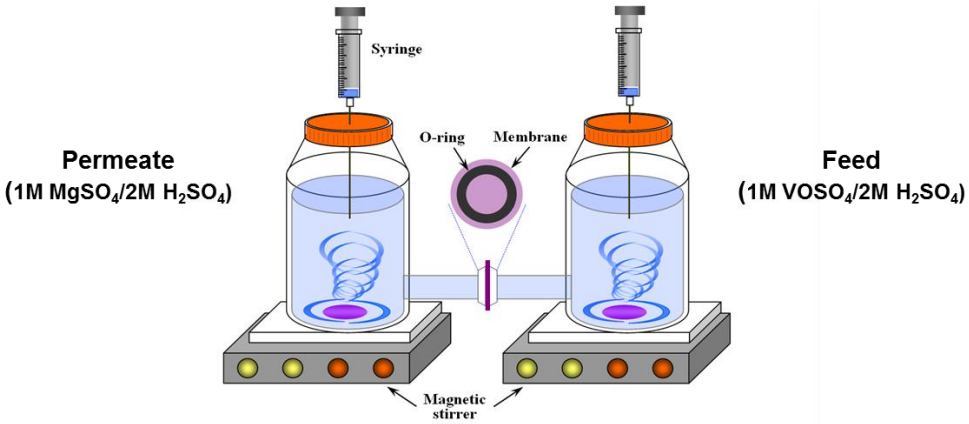


**Fig 4. Schematic representation of vanadium glass diffusion cell.**

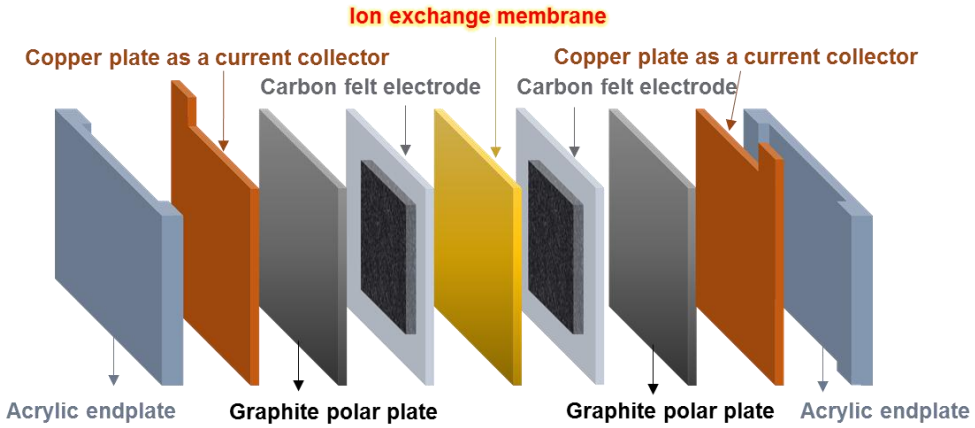


**Fig 5. Schematic diagram of a VRB single cell.**

# 3. Results and Discussion

## 3.1. Characteristics of ETS-10

### 3.1.1. Crystallinity and morphology of ETS-10

Table 1 shows the synthesis condition and sample code. Fig 6 shows the X-ray diffraction patterns of byproducts with various conditions. The XRD pattern of synthesized particles showed the main peak of ETS-10. However, the particles synthesized with some conditions showed the quartz peak at 22° and 27°. These result comes from the dissolved degree of silica source. When silica source is not dissolved enough, it forms the quartz phase. The XRD pattern of synthesized using $TiO_2$ (anatase) showed the anatase peak at 25.5°. The XRD pattern of synthesized using P25 is in agreement with literature and shows the material is highly crystalline and free of by-products. Fig 7 shows the SEM results of byproducts with various conditions. The size of ETS-10 particle using TIP and $TIO_2$ and P25 is around 20 μm, 1 μm and 500 nm, respectively. The particle size difference between ETS-10 using $TiO_2$ and that using P25 comes from the particle size of titanium source. The size of $TiO_2$ (anatase) is around 200 nm, while that of P25 is around 40 nm.

Fig 8 shows the FT-IR spectrum of an ETS-10 powder synthesized using P25. Vibration-band assignments for the infrared spectrum of ETS-10 are available in the literature [38]. The high-frequency region of the ETS-10 spectrum shows a sharp split peak at about 1650 $cm^{-1}$, which is attributed to the scissoring modes of the absorbed water molecules. The band around 1000 $cm^{-1}$ is dominated by Si-O bond stretching modes, which generate a strongly intense band. The peak from 400 to 800 $cm^{-1}$ is determined by both Ti-O and Si-O modes. The crystallinity and size of ETS-10 using P25 and colloidal silica source is suitable synthesis condition for the dispersion in the polymer matrix without precipitation.

| Ti Precursor | Si Source | Temperature (°C) | Sample code |
|---|---|---|---|
| Titanium isopropoxide (TIP) | Sodium silicate solution | 200 | TIP_SS_200 |
| | | 230 | TIP_SS_230 |
| | Colloidal silica | 200 | TIP_CS_200 |
| | | 230 | TIP_CS_230 |
| $TiO_2$ (anatase) | Sodium silicate solution | 200 | TIO_SS_200 |
| | | 230 | TIO_SS_230 |
| | Colloidal silica | 200 | TIO_CS_200 |
| | | 230 | TIO_CS_230 |
| P25 (anatase, rutile) | Sodium silicate solution | 200 | P25_SS_200 |
| | | 230 | P25_SS_230 |
| | Colloidal silica | 200 | P25_CS_200 |
| | | 230 | P25_CS_230 |

**Table 1. Synthesis condition and sample code.**

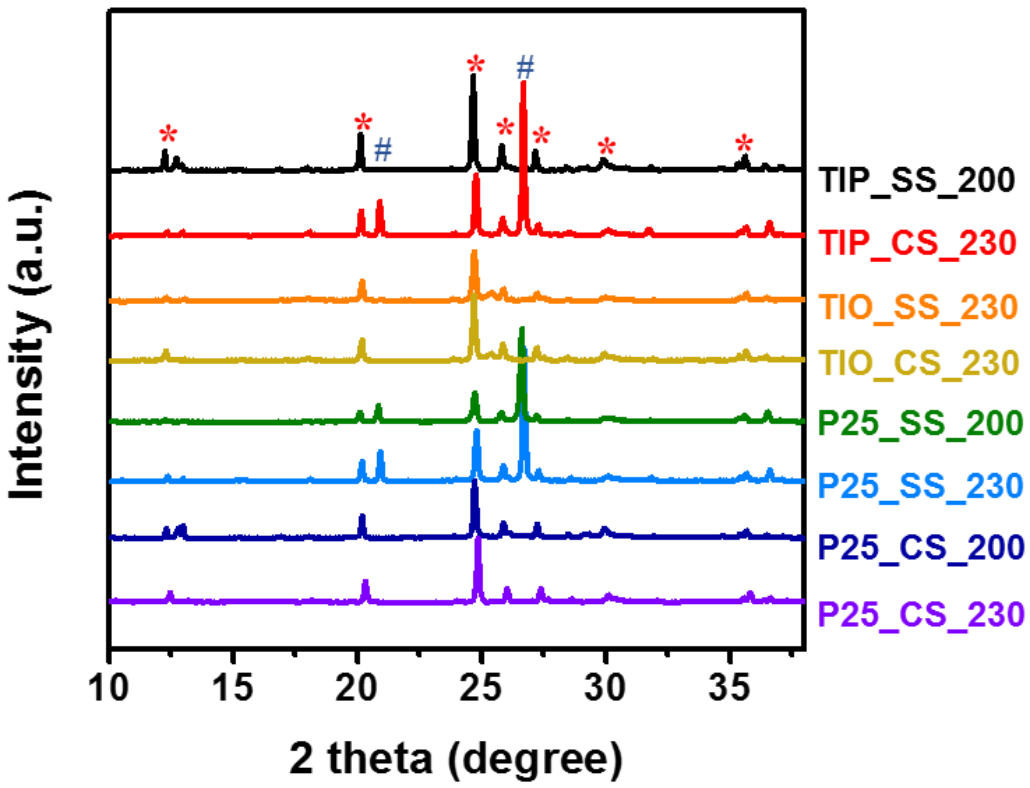


**Fig 6. XRD patterns of the ETS-10 particle with various synthesis condition (* : main peak of ETS-10, # : quartz peak).**

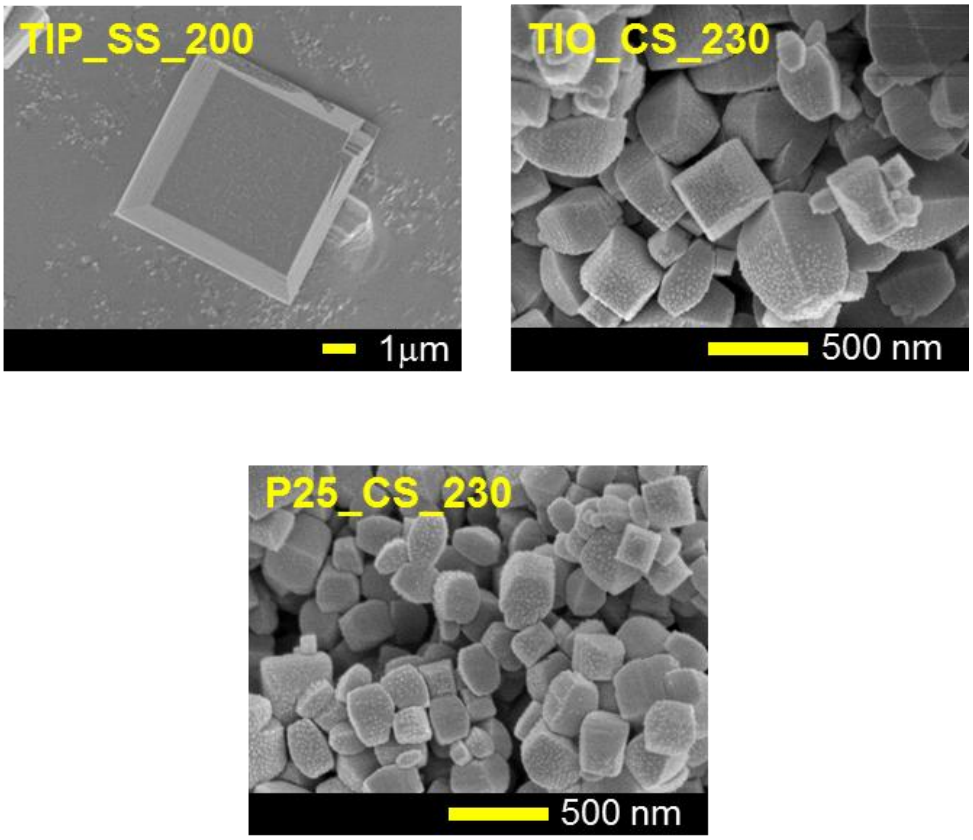


**Fig 7. FE-SEM images of the ETS-10 particles.**

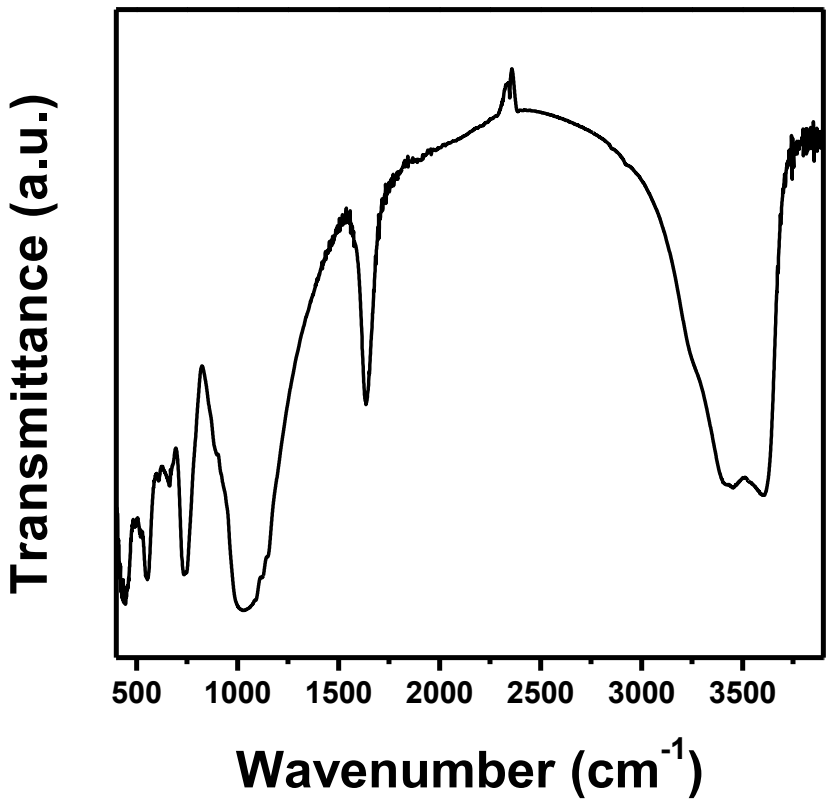


**Fig 8. FT-IR spectrum of optimum ETS-10 in the wavenumber range of 400 – 3800 $cm^{-1}$.**

### 3.1.2. Acid resistance of ETS-10

To clarify the acid resistance of ETS-10 particle, acid tolerance test was conducted at 2M $HSO_4$ aqueous solution, which is the VRB electrolyte condition. Synthesized particles were placed in the acid solution. After a given period of time, the particles were recovered by centrifugation. The result of the test is illustrated in Fig 9. After acid treatment, some main peaks of ETS-10 were intensified (12 °, 18 °, 24 °, 25 °, 26 °) and other peaks were weakened (27 °, 30 °, 36 °). It can be explained by the transformation of outer surface and ion exchange. First, when ETS-10 particles are exposed to acid solution, proton attacks exposed Ti-O-Ti bonds and forms the Ti-OH bond. Second, ETS-10 contains guest ion at its framework. When it contact other cations such as proton, ion exchange occur. The XRD peak of ETS-10 can be changed by the ion exchange because the size of cations is different. Furthermore, impurity can be removed during acid-treatment. It can cause the increment of crystallinity resulting in higher intensity of main peaks. Consequently, synthesized ETS-10 have the acid resistance in VRB electrolyte condition.

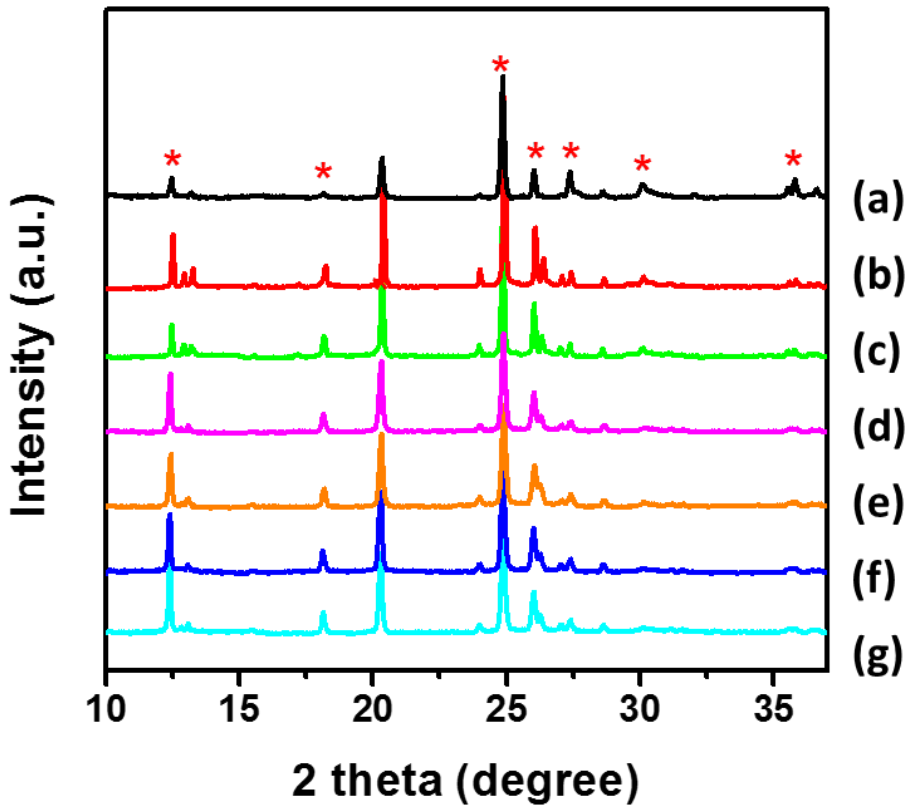


**Fig 9. XRD patterns of ETS-10 particles in 2 M sulfuric acid**

**(* : main peak of ETS-10)**

**(a) : as-synthesized ETS-10, (b) : after 6 hours, (c) : after 1 day,**

**(d) : after 2 weeks, (e) : after 1 month, (f) : after 3 months,**

**(g) : after 6 months.**

### 3.2.Characterization of SPEEK/ETS-10 composite membrane

#### 3.2.1. Membrane morphology study

Fig 10 shows a cross-sectional FE-SEM image and the corresponding energy dispersive spectroscopy (EDS) mapping of composite membranes. The FE-SEM image confirmed that there are no cracks in membranes. The EDS titanium mapping images given in Fig 11 show that ETS-10 particle disperse homogeneously throughout the cross-section of the membranes. Upon increasing ETS-10 contents in the composite membranes, the titanium distribution gradually increases. These results comes from hydrophilicity and suitable particle size of ETS-10 particles.

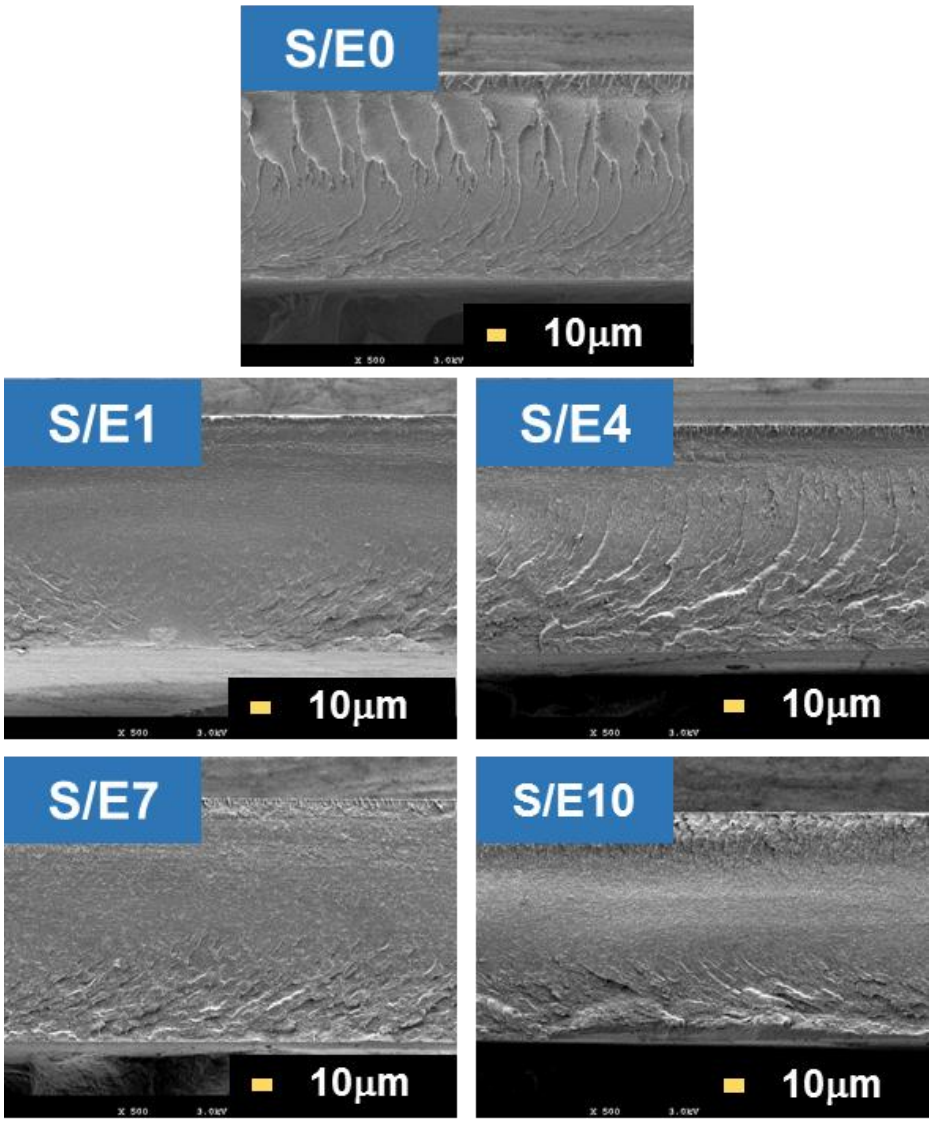


**Fig 10. FE-SEM cross-section images of S/E membrane.**

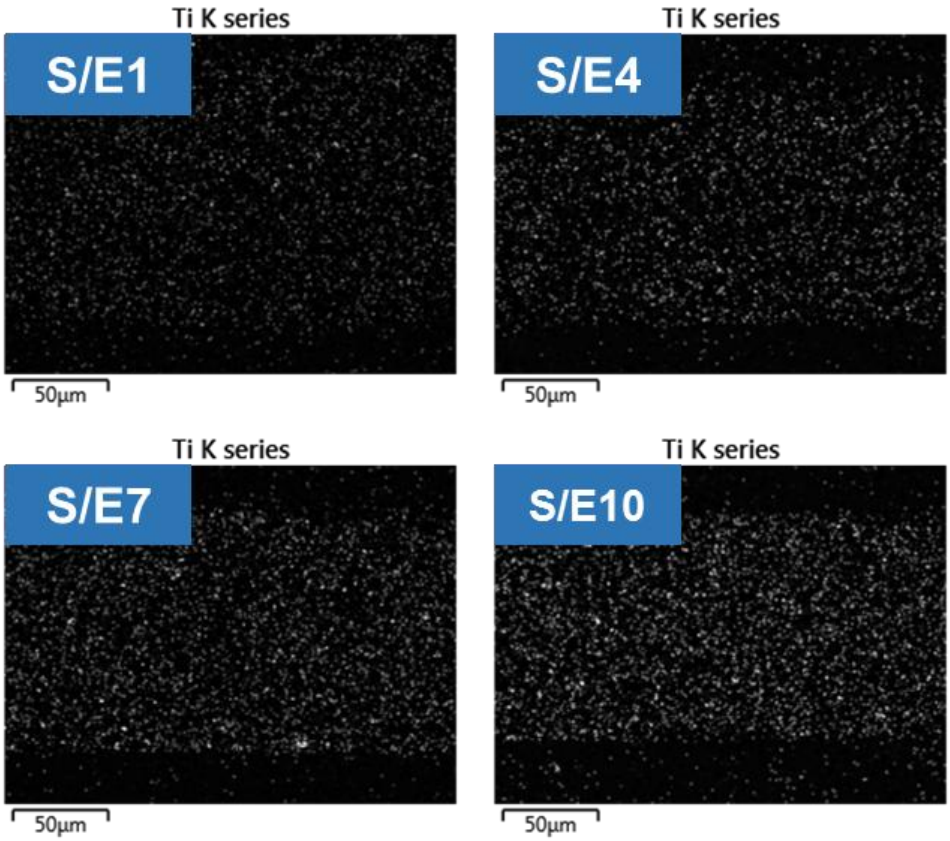


**Fig 11. EDS cross-section images (Ti source mapping)**

**of S/E series membranes.**

### 3.2.2. Physicochemical properties

Fig 12 and Fig 13 show the water uptake and ion exchange capacity of pristine SPEEK membranes and SPEEK/ETS-10 composite membrane measured at room temperature respectively. The water uptake of the membranes was found to increase as ETS-10 contents, owing to the hydrophilic nature of ETS-10.

The ion exchange capacity of the S/E composite membrane is higher than that of Nafion117 membrane owing to the high degree of sulfonation. The ion exchange capacity of the composite membrane shows slightly increase as ETS-10 particle loading. It can be explained by high ion exchange capacity of the ETS-10 using micropore. When the membranes placed in the aqueous solution, water molecules are absorbed by not only SPEEK polymer containing $SO_3^-$ functional group but also ion exchangeable micropore of ETS-10 particles. Overall, this indicates that ETS-10 can effectively change the properties of the absorption of water molecules and protons.

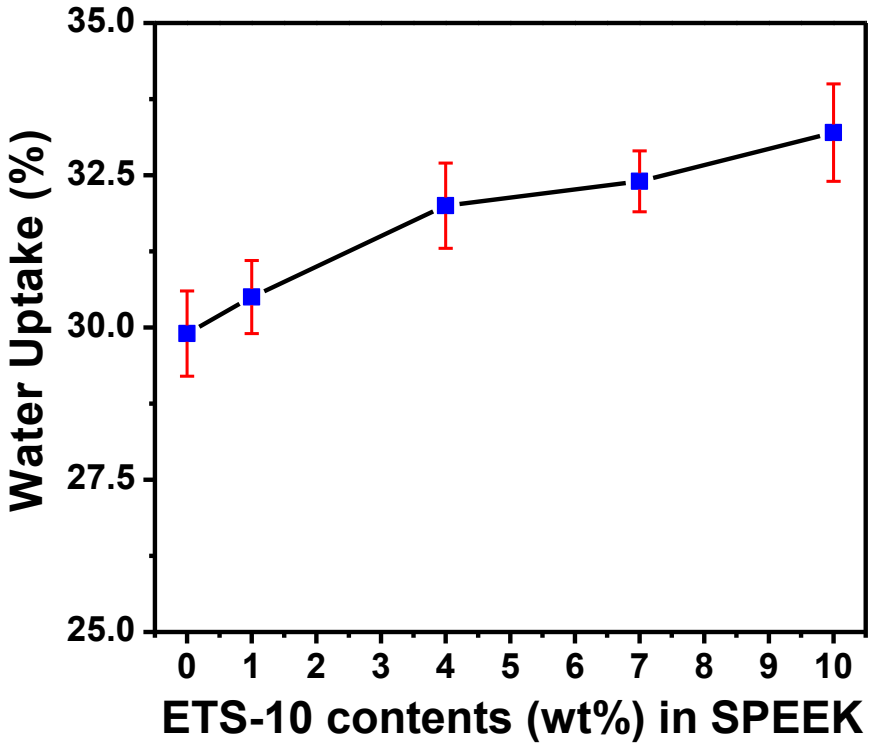


**Fig 12. Water uptake for S/E composite membrane as function of ETS-10 content.**

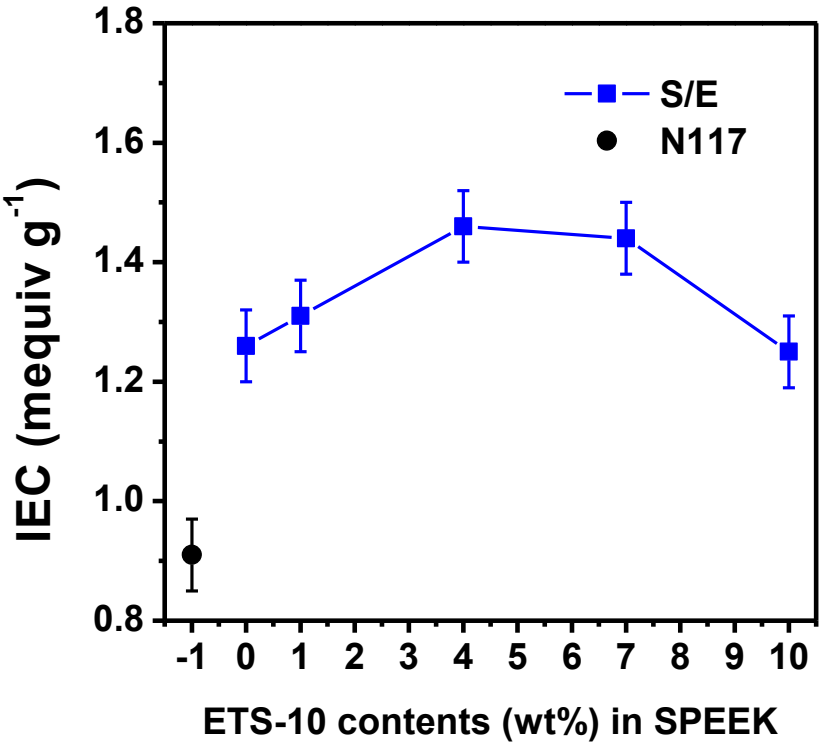


**Fig 13. IEC for N117 membrane and S/E composite membrane as function of ETS-10 content.**

### 3.2.3. Mechanical properties

Table 2 shows the mechanical properties of Nafion 117 and composite membranes. It can be seen that the young's modulus and tensile strength at maximum load of composite membranes are higher than Nafion 117 membrane, indicating that SPEEK and SPEEK/ETS-10 composite membrane have better mechanical property than Nafion 117 membrane. It can be due to the robust aromatic backbone of SPEEK, while Nafion 117 membrane has flexible aliphatic main chain. The tensile strength and young's modulus increase with increasing ETS-10 contents, which can be attributed to the uniform distribution of ETS-10 particle in the SPEEK matrix and the interaction between sulfonic acid group on SPEEK and hydroxyl group on ETS-10 particle surface.

**Table 2. Mechanical properties of N117 and S/E composite membrane**

| | N117 | S/E0 | S/E1 | S/E4 | S/E7 | S/E10 |
|---|---|---|---|---|---|---|
| Tensile stress (MPa) | 19.1 | 12.0 | 15.6 | 23.3 | 18.6 | 17.0 |
| Young's modulus (MPa) | 331.6 | 565.8 | 585.0 | 682.2 | 737.1 | 792.9 |

### 3.2.4. Proton conductivity

The impedance spectroscopy results and the proton conductivity are shown in Fig 14 and Fig 15, respectively. S/E1 (41.08 mS $cm^{-1}$) and S/E4 (40.01mS $cm^{-1}$) shows higher proton conductivity than SPEEK (37.67 mS $cm^{-1}$). The proton conductivity of other composite membranes decrease as further particle loading. There is no proton conductivity loss up to 4wt% of ETS-10 contents. These result comes from hydrophilicity and micropore of ETS-10. As mentioned above, ETS-10 have high hydrophilicity due to abundant surface –OH group. Furthermore, ETS-10 can absorb water molecular in micropore. Therefore, proton conductivity increase because water molecular act as a hopping site. On the other hand, as reported in the literature [39], hydrophilic zeolites have a lot of extra-framework cations. In the hydrated state, acceptor sites (-δ) in anionic zeolite framework can be facilitated for proton mobility. These negatively charged vacancies promotes proton transport inside of framework. Consequently, the proton conductivity loss is minimized due to new pathway provided by micropore, although the proton migration through ionic cluster channel is disturbed by tortuous pathway effect. Decrease of the proton conductivity at further ETS-10 loading can be explained by the fact that

when high ETS-10 loading, tortuosity of proton transport increase. These effect is superior to proton migration through ETS-10 effect in the proton conductivity. One can assume that at high loadings, the formation of ETS-10-particle aggregates induces partial phase separations and interrupts of connection of ionic cluster channel.

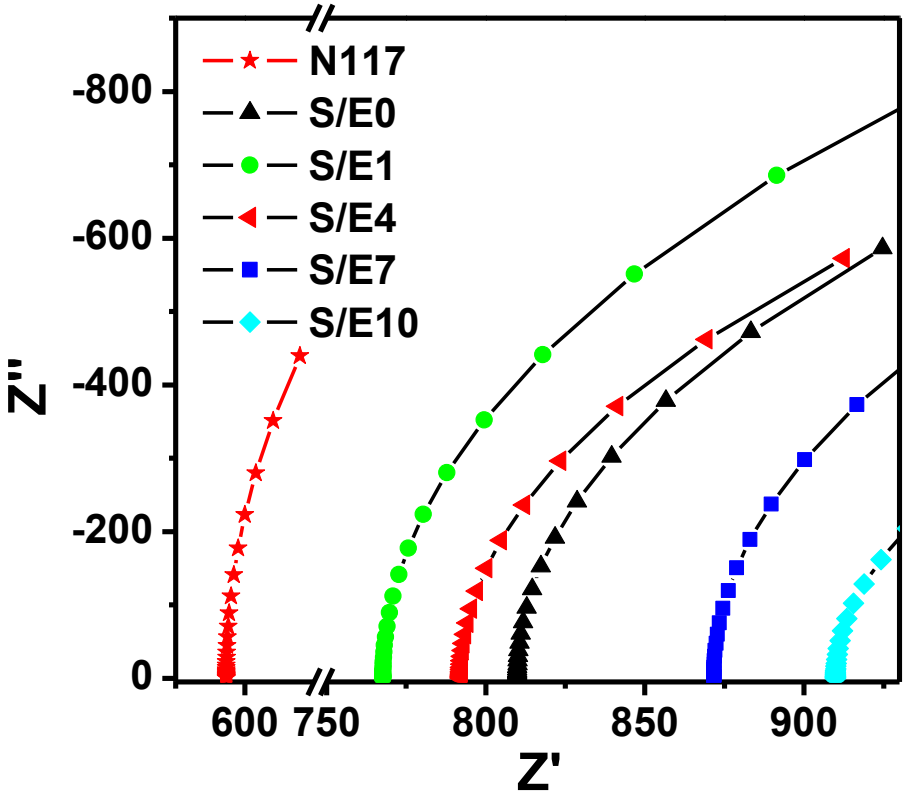


**Fig 14. Impedance spectroscopy for N117 and S/E composite membrane (Nyquist plot).**

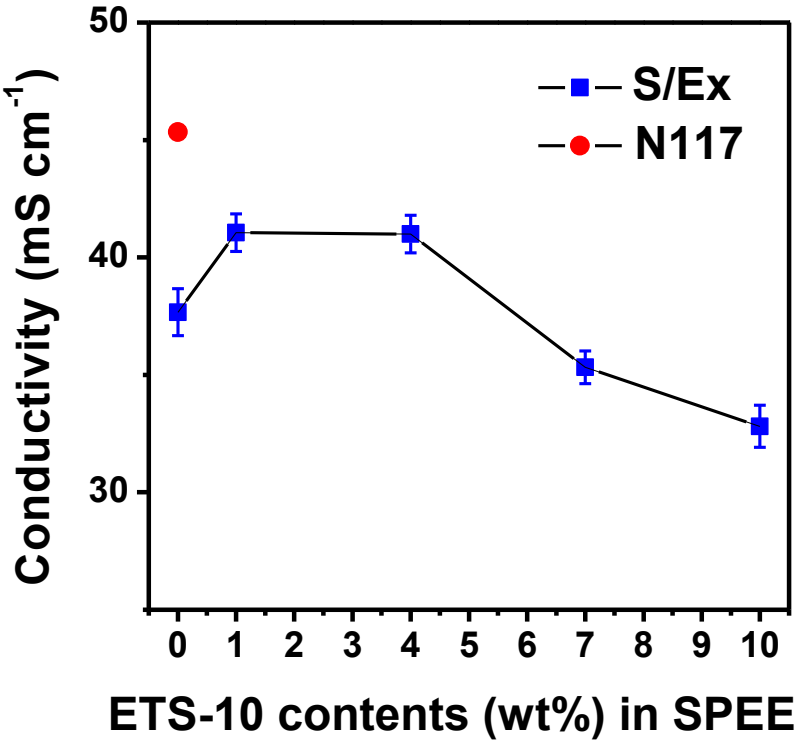


**Fig 15. Proton conductivity of N117 and S/E series composite membranes fabricated with different ETS-10 contents.**

### 3.2.5. Vanadium ion permeability and ion selectivity

The vanadium concentration in the compartment of diffusion cell is shown in Fig 16 as a function of time for N117 and various SPEEK/ETS-10 composite membranes with ETS-10 content. A relationship between $VO^{2+}$ concentration and time is linear. After the same time interval, concentration of $VO^{2+}$ of permeate compartment using SPEEK/ETS-10 membrane is lower than that using SPEEK and N117. According to the equation provided in above, vanadium permeability are illustrated in Fig 17. It is found that $VO^{2+}$ permeability across the membranes decrease as ETS-10 loading. It can be explained by permselectivity of micropore and tortuous pathway effect. The multi-hydrated vanadium ion transport through zeolite particle is much hindered by framework of ETS-10 than hydronium ion transport because hydronium ion have smaller ion radius than multi hydrated vanadium ion. Therefore vanadium ion transport is delayed kinetically. On the other hand, the vanadium ion have to follow a more tortuous path around the ETS-10 particles. As ETS-10 particle loading, the vanadium permeability decrease because tortuosity of the vanadium ion increase.

Fig 18 shows the ion selectivity of S/E series composite membranes as a function of ETS-10 contents. The selectivity increase as ETS-10 loading up to 4 wt% due to the low vanadium permeability and improved proton conductivity. S/E7 and S/E10 membranes shows lower ion selectivity than S/E4 membrane despite the low vanadium permeability. It comes from the fact that proton conductivity is sharply decrease above 4 wt% loading.

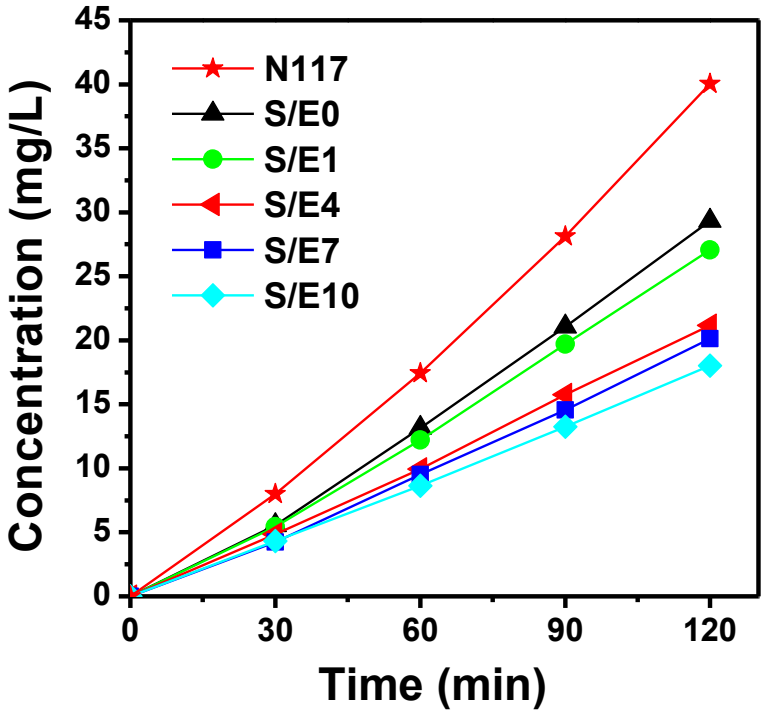


**Fig 16. Vanadium concentrations in water compartment with various times for S/E composite membranes.**

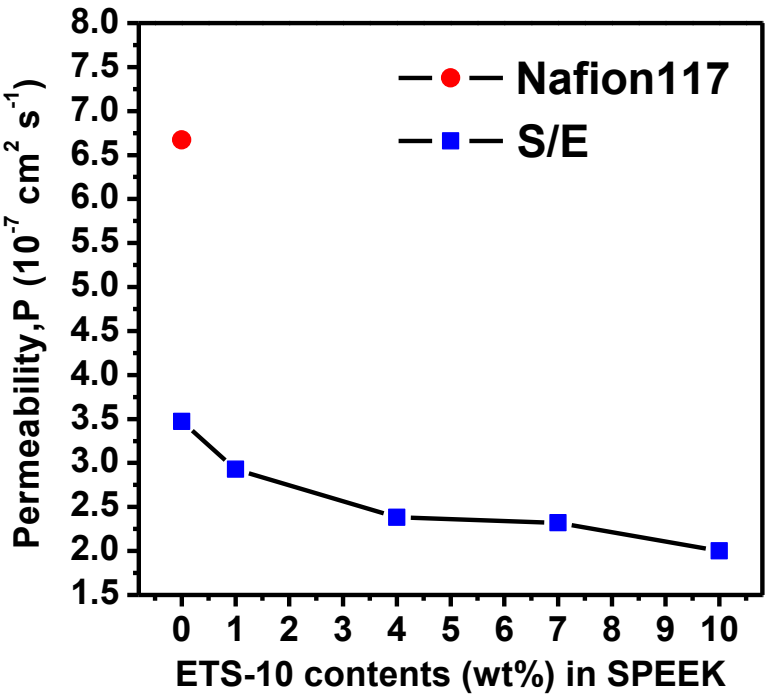


**Fig 17. Variation of vanadium permeability of S/E series composite membranes according to ETS-10 contents.**

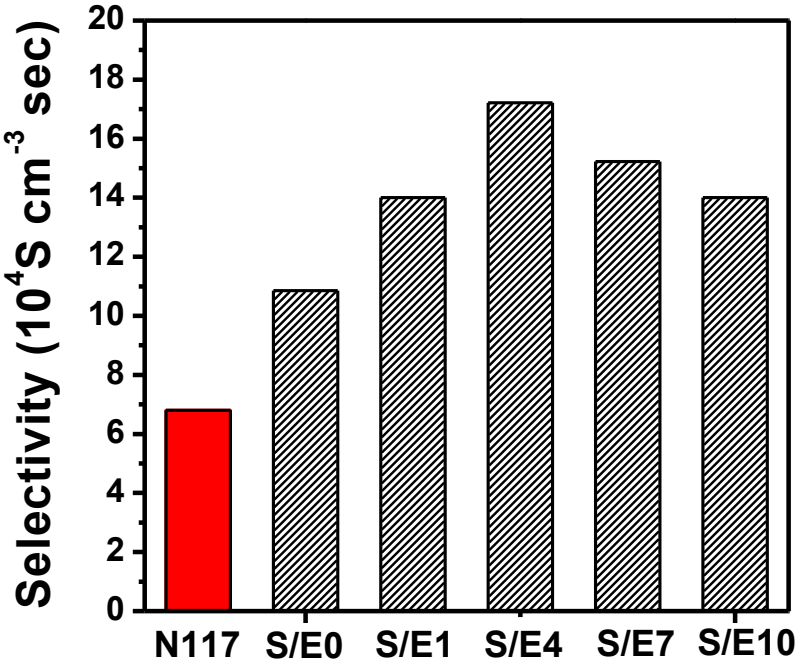


**Fig 18. Ion selectivity of N117 membrane and S/E series composite membrane.**

### 3.2.6. VRB single cell performance

The charge-discharge curves of VRBs with Nafion117, S/E0, S/E1, S/E4, S/E7, S/E10 membranes at the current density of 40, 60, 80, 100 mA $cm^{-2}$ are illustrated in Fig 19. The rank of charge and discharge capacity of membranes is S/E4 > S/E1 > S/E0 > N117 > S/E7 > S/E10 at 80 mA $cm^{-2}$. The capacity of the membranes increase as ETS-10 loading up to 4 wt%, indicating that the crossover of vanadium ion is suppressed by loading ETS-10 particle. However, S/E7 and S/E10 show lower capacity than other samples. As shown in above area resistance result, S/E7 and S/E10 shows higher membrane resistance. It lead to higher voltage during charge procedure, and lower voltage during discharge procedure. Therefore, the VRB cell using S/E7 and S/E10 can reach the setup voltage earlier compared to other samples which have low membrane resistance.

Fig 20 shows the result of the charge-discharge test with various membranes at different current densities to confirm coulombic efficiency (CE), voltage efficiency (VE) and energy efficiency. The rank of CE is S/E10 > S/E7 > S/E4 > SPE1 > S/E0 at 80 mA $cm^{-2}$, in accordance with the results on vanadium ion permeability. With the increasing of ETS-10 contents, the $VO^{2+}$ permeability of composite

membranes decreases, leading to lower cross-mixing of vanadium ions and higher CE. The CE of Nafion117 was lower than S/E4, S/E7, S/E10 at all current densities.

The VE has an order of S/E4 > S/E1 > S/E0 > S/E7 > S/E10 at 80 mA $cm^{-2}$. This can be explained by the results of proton conductivity. Because there is no conductivity loss at S/E1 and S/E4, they showed higher VE compared to S/E0, pristine SPEEK. The VE of Nafion117 is lower than S/E1 and S/E4. It can be due to the difference of thickness between Nafion117 (210 $\mu$m) and S/E (120 $\mu$m). The proton pathway through Nafion117 is longer than that through S/E. Therefore, Nafion117 has lower VE although it has the qualitatively highest ion conductivity.

The EE indicate the energy conversion ability for large-scale VRB system. The rank of EE is S/E4 > S/E1 > S/E0 > S/E7 > S/E10 at 80 mA $cm^{-2}$. The EEs of S/E4 and S/E1 are higher than that of other membranes at all current densities due to low vanadium-crossover without proton conductivity loss. In spite of low vanadium ion permeability, the EE of S/E7 and S/E10 is lower than other membranes, resulting from their high area resistance. The S/E4 showed the best single cell performance of CE (99%), VE (80.0%) and EE (79.2%) at

80 mA $cm^{-2}$, while the Nafion117 shows the cell performance of CE (98.8%), VE (72.3%) and EE (71.4%).

The charge-discharge tests for VRBs with Nafion117 and S/E4 membranes over 100 cycles are compared in Fig 21. The EEs of the cell with S/E4 and S/E0 remained nearly constant during 100 cycles, while that of the cell with Nafion118 decrease from 81.3% to 76.8%, indicating that SPEEK membrane showed a stable performance in vanadium solution under strongly acidic conditions compared to Nafion117. Fig 22 shows the capacity loss curves of the VRB cell with Nafion117 and S/E4. The S/E4 membrane has lower capacity loss ratio than Nafion117 over 100 cycles, which can be due to its lower vanadium ion permeation. After 100 cycles, S/E4 membrane sustains 76.2% of first cycle discharge capacity while Nafion117 membrane remains only 68.1%. Consequently, the cycle test of two membranes conclude that the S/E4 composite membrane exhibit high single cell performance and good stability in VRB.

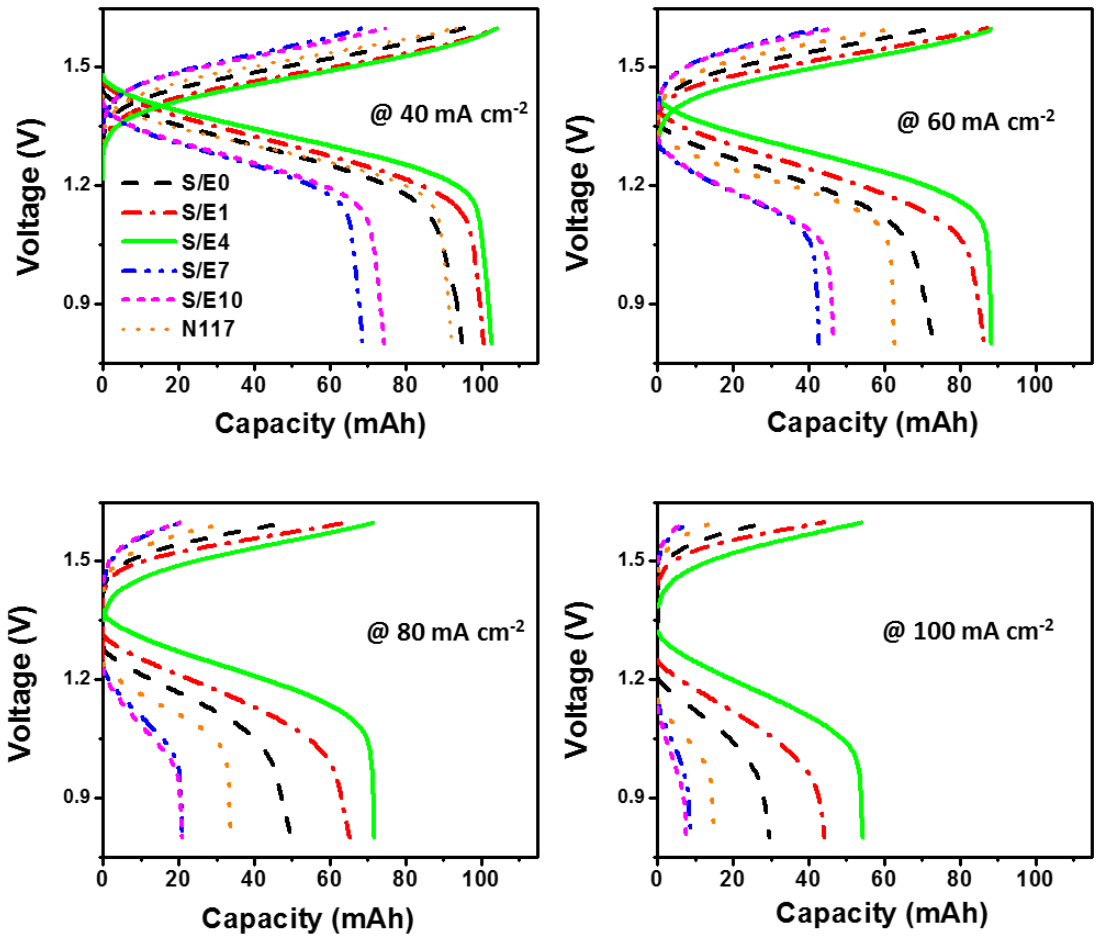


**Fig 19. Charge-discharge curves of VRBs with N117 and S/E series composite membranes at 40, 60, 80, 100 mA cm$^{-2}$.**

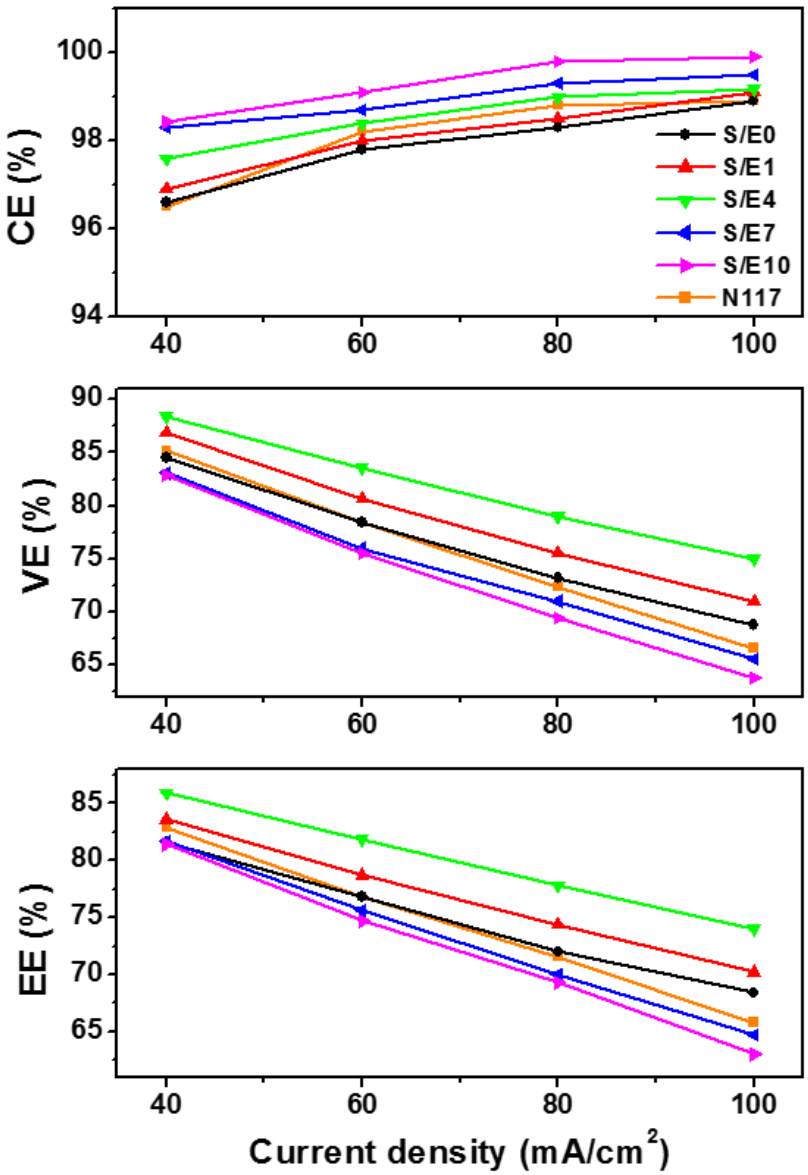


**Fig 20. Cell performance of VRBs with N117 and S/E series membranes under different current densities.**

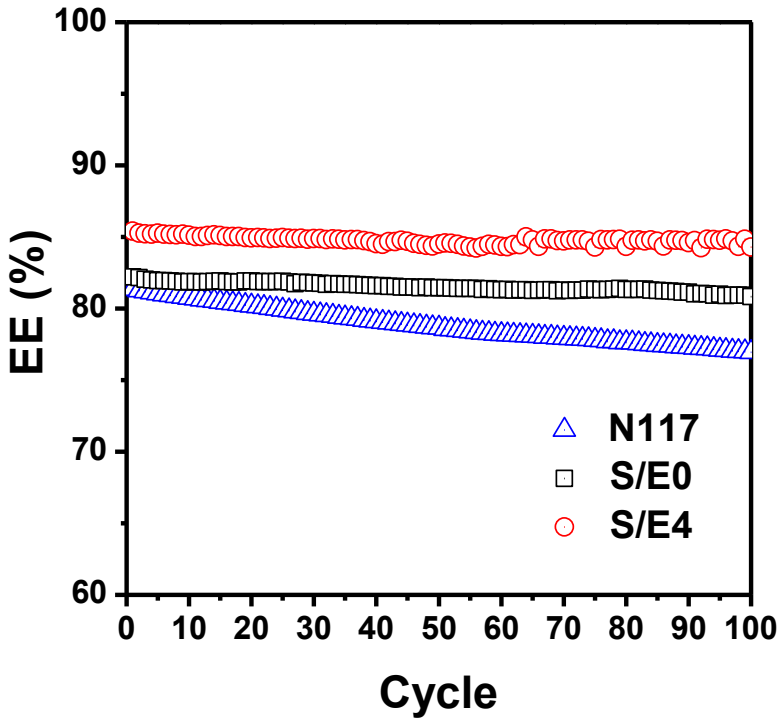


**Fig 21. Variation of energy efficiency of VRBs with N117, S/E0 and S/E4 membranes during 100 cycles.**

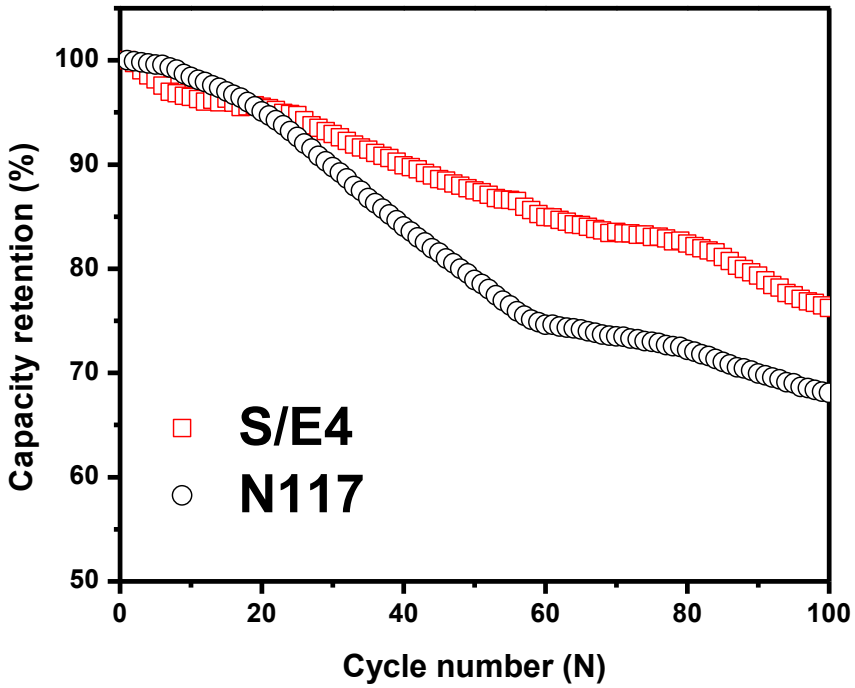


**Fig 22. Capacity retention of VRBs with N117 and S/E4 membranes during 100 cycles.**

### 3.3. Characterization of SPEEK/ETS-10@PTFE membrane

#### 3.3.1. Membrane morphology study

The FE-SEM images and the energy dispersive spectroscopy (EDS) mapping images of membrane cross-section are showed in Fig 23. Thickness of the membrane is around 70 μm, while that of S/E series membrane is around 120 μm. The FE-SEM image showed that the cross-section of membranes is relatively tough due to PTFE fiber. The EDS sulfur mapping images showed that SPEEK polymer densely fills the pore of PTFE. To clarify the mass ratio of SPEEK in PTFE, TGA results are shown in Fig 24. The mass ratio of SPEEK polymer in SPEEK/PTFE is 81%. The EDS titanium mapping images given in Fig 25 shows that ETS-10 particle disperse homogeneously throughout the membranes. Upon increasing ETS-10 contents, the titanium mapping gradually increases. However, the membrane containing ETS-10 particle over 4 wt% showed the deposition of particle at surface.

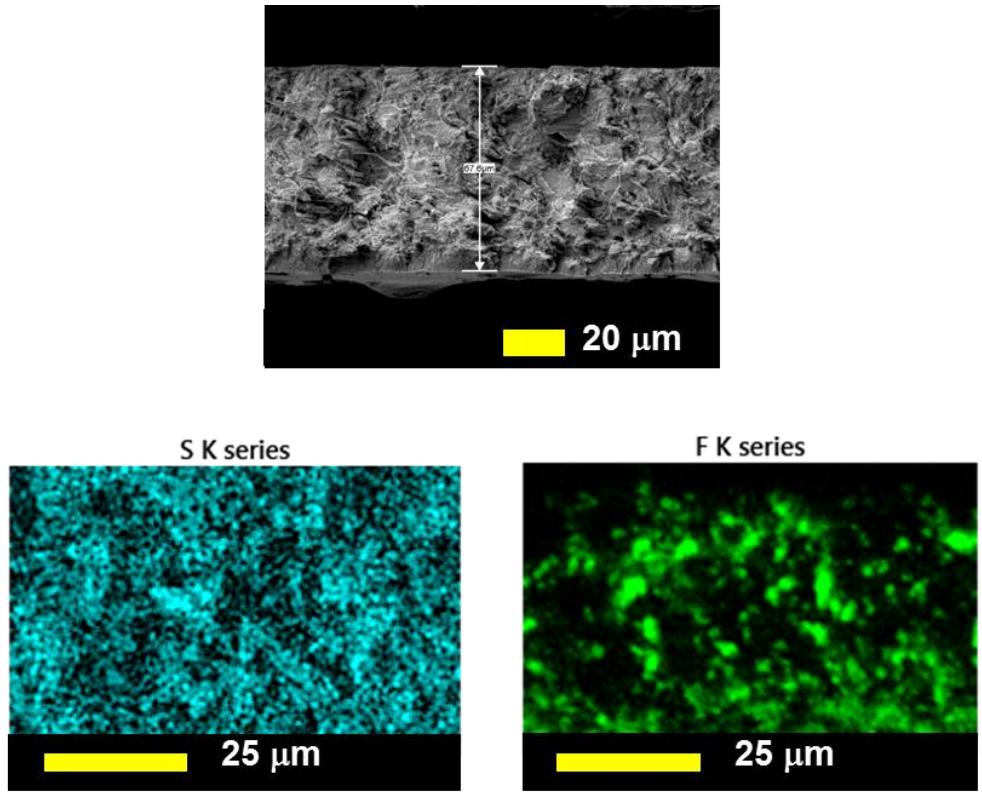


**Fig 23. FE-SEM and EDS cross-section images of S/E@P0 membrane.**

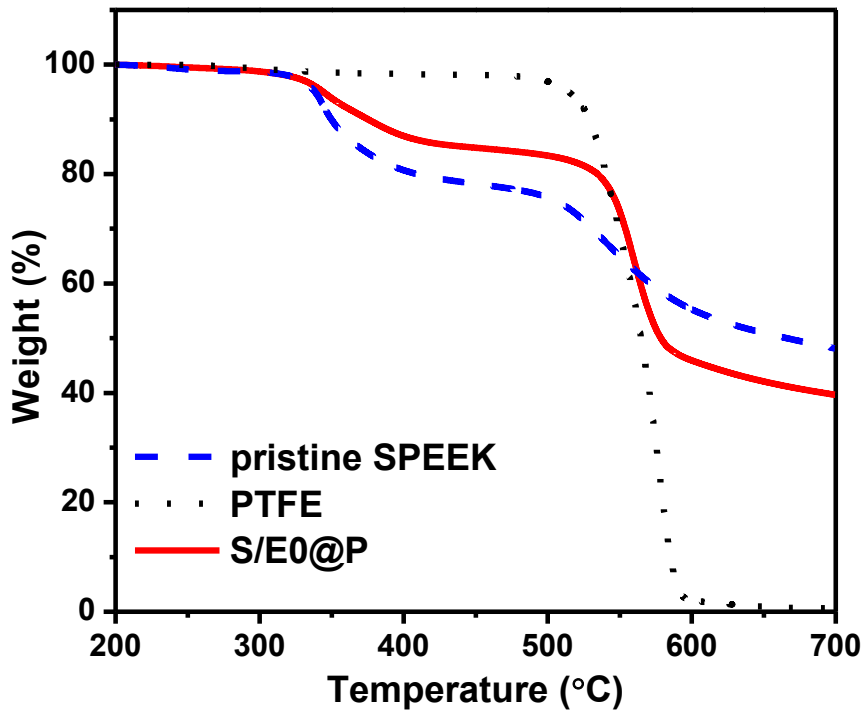


**Fig 24. TGA results for SPEEK, PTFE and S/E0@P membranes**

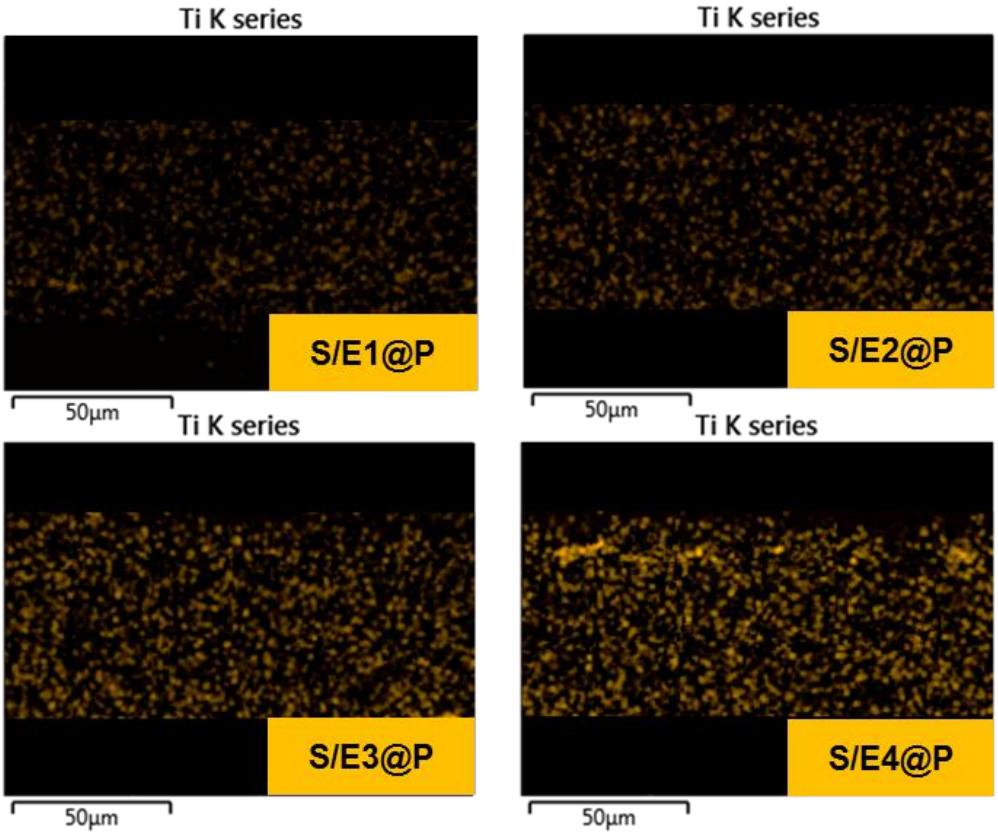


**Fig 25. EDS cross-section images (Ti source mapping)**

**of S/E@P series membranes.**

### 3.3.2. Physicochemical properties

Fig 26 shows the water uptake and swelling ratio of pristine SPEEK membranes and pore-filled membranes measured at room temperature. The water uptake gradually increases as ETS-10 loading. Pore-filled membranes showed lower water uptake than pristine SPEEK

The swelling ratio is related to the chemical and mechanical stability of membranes. Pore-filled membranes showed lower swelling ratio than pristine SPEEK. The results of water uptake and swelling ratio of pore-filled membrane are attributed to PTFE matrix. The PTFE matrix is not able to absorb the water and swell. Because the swelling of ion exchangeable polymer is confined by the PTFE matrix, water uptake and swelling ratio are reduced compared to pristine SPEEK.

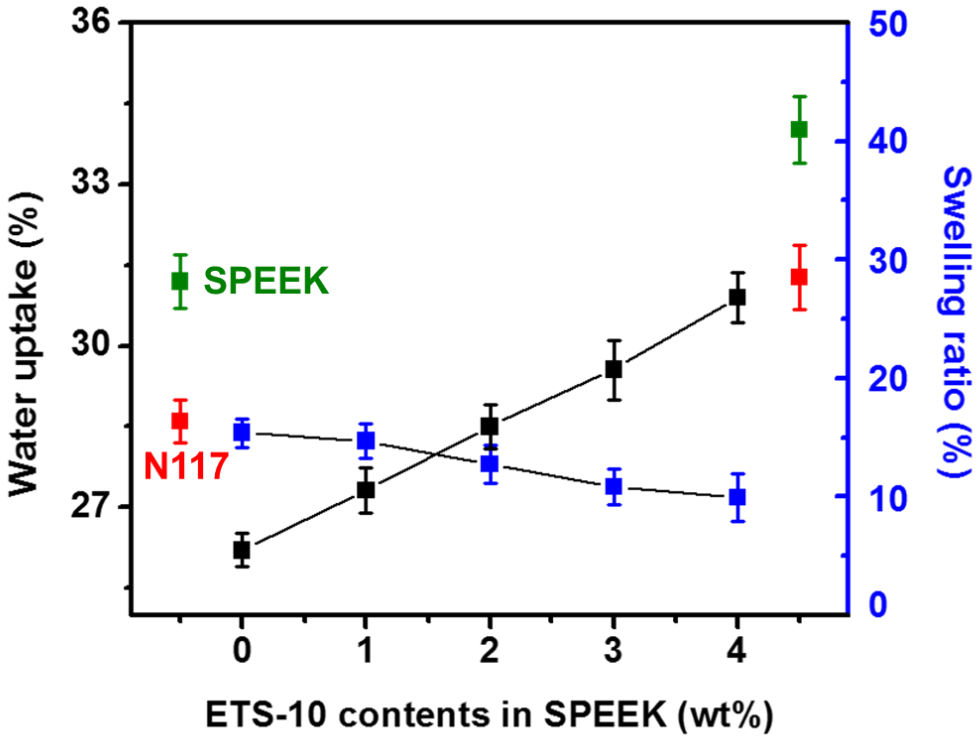


**Fig 26. Water uptake and swelling ratio for N117, SPEEK and S/E@P series membranes**

### 3.3.3. Mechanical properties

Table 3 shows the mechanical properties of Nafion 117, pristine SPEEK and pore-filled membranes. The tensile stress of the pore-filled membranes are gradually increase and the elongation at break decrease as ETS-10 loading up to 3 wt%, resulting from the fact that addition of inorganic particle can make membrane rigid. In case of S/E4@P, containing 4 wt% ETS-10 particles, tensile stress decrease. It can be assumed that deposition and aggregation part of ETS-10 particles can act as a cracking point to membrane.

It can be seen that S/E3@P membrane exhibit the good mechanical behavior. The maximum tensile strength of the membrane can reached up to 50 MPa, which is higher than that of Nafion117 (19 MPa) and pristine SPEEK (12 MPa). It can be confirmed that PTFE matrix can reinforce the membrane. Therefore, S/E3@P membrane is acceptable for application in assembly of VRB system despite their low thickness.

**Table 3. Mechanical properties of N117 and S/E@P series membrane**

| | N117 | S/E0@P | S/E1@P | S/E2@P | S/E3@P | S/E4@P |
|---|---|---|---|---|---|---|
| Tensile stress (MPa) | 19.1 | 34.4 | 39.1 | 42.0 | 49.5 | 42.9 |
| Young's modulus (MPa) | 331.6 | 876.8 | 932.6 | 985.3 | 1197.7 | 1253.5 |

### 3.3.4. Proton conductivity

The impedance spectroscopy result is shown in Fig 27 for S/E@P pore-filled membranes. The charge transfer resistance of the membranes decrease as ETS-10 loading up to 2 wt% and further loading of ETS-10 lead to the resistance increase. All of pore-filled membrane containing ETS-10 particles shows lower resistance than S/E0@P.

On the basis of the impedance spectroscopy results, the proton conductivity is calculated and shown in Fig 28. S/E2@P and S/E3@P membrane show improved proton conductivity compared to S/E0@P membrane. Furthermore, the conductivity value is comparable to that of Nafion117. The results can be explained by high sulfonation degree of SPEEK and effect of ETS-10. As mentioned above at S/E series, the hydrophilicity of ETS-10 and micropore can facilitate the proton conduction.

Overall, the conductivity of membranes is lower than pristine SPEEK membrane and their low thickness can be a further advantage for proton conduction.

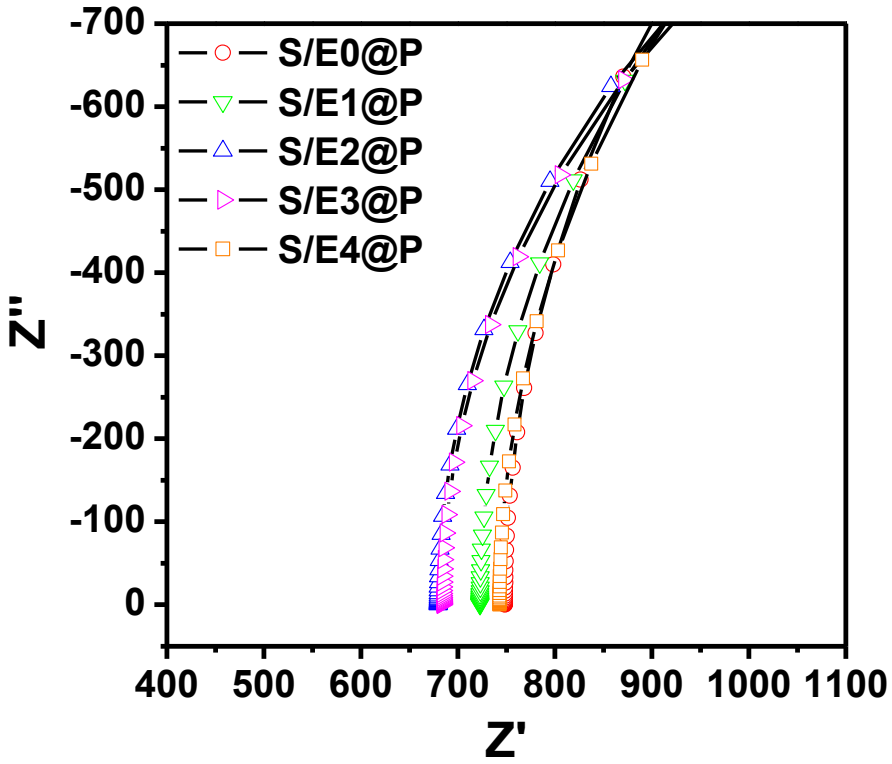


**Fig 27. Impedance spectroscopy for N117 and S/E@P series membrane (Nyquist plot)**

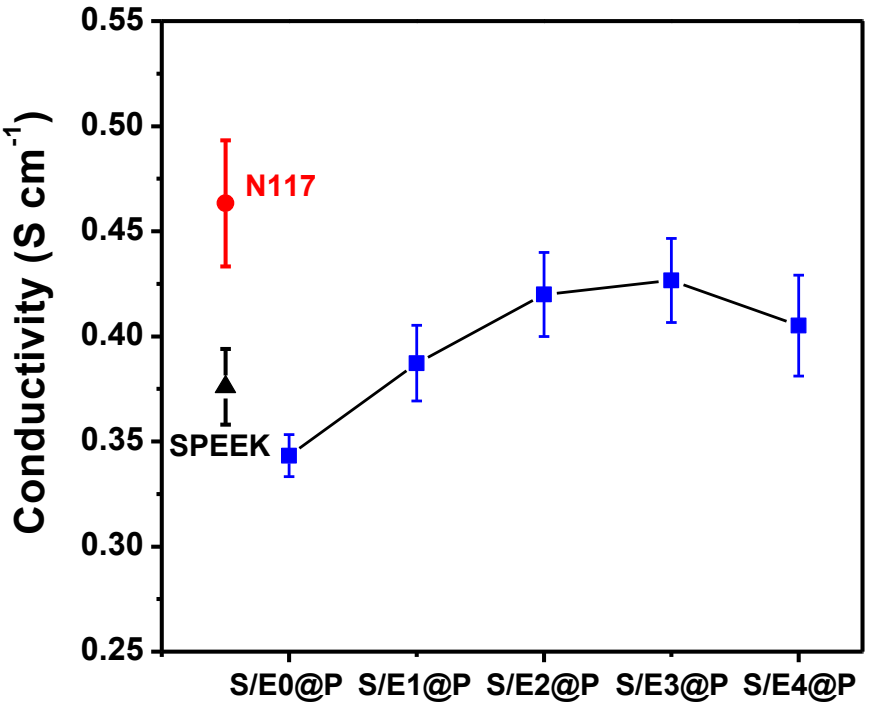


**Fig 28. Proton conductivity of N117, SPEEK and S/E@P series membranes fabricated with different ETS-10 contents.**

### 3.3.5. Vanadium permeability and ion selectivity

The vanadium concentration in the compartment of diffusion cell is shown in Fig 29 as a function of time for N117 and various S/E@P pore-filled membranes. A relationship between $VO^{2+}$ concentration in the compartment of diffusion cell and time is nearly linear. After the same time interval, concentration of $VO^{2+}$ of permeate compartment using S/E@P membrane is lower than that using N117. According to the equation provided in above, vanadium permeability of the membranes is shown in Fig30. It can be found that the $VO^{2+}$ permeability across the pore-filled membranes is lower than pristine SPEEK and Nafion117. It can be due to the PTFE matrix The PTFE matrix confine the swelling of membrane, resulting in narrow the ionic channel and the transport of multi-hydrated vanadium ion can be interrupted. Furthermore, among the pore-filled membranes, the $VO^{2+}$ permeability decrease as ETS-10 loading. As mentioned above, it can be due to the permselectivity of micropore and tortuous pathway effect of ETS-10. The size difference between the multi-hydrated vanadium ion and hydronium ion can widen the difference of diffusion rate through micropore or tortuous pathway induced by ETS-10 particles.

Selectivity is a key factor for evaluating membrane performance in a roundabout way, which defined as the ratio of proton conductivity over vanadium permeability. In Fig 31, the S/E3@P membrane shows a selectivity of 5.67 $\times 10^8$ S $cm^{-3}$ sec, which is about six times higher than that of Nafion 117 membrane (0.87 $\times 10^8$ S $cm^{-3}$ sec).

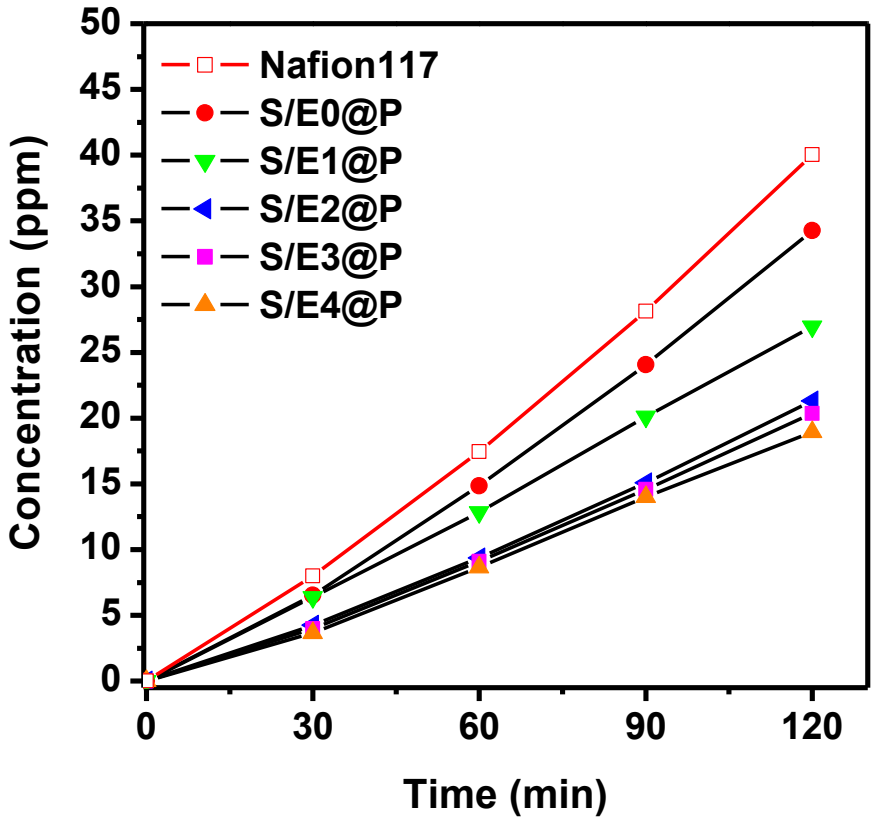


**Fig 29. Vanadium concentrations in water compartment with various times for N117 and S/E@P series membranes.**

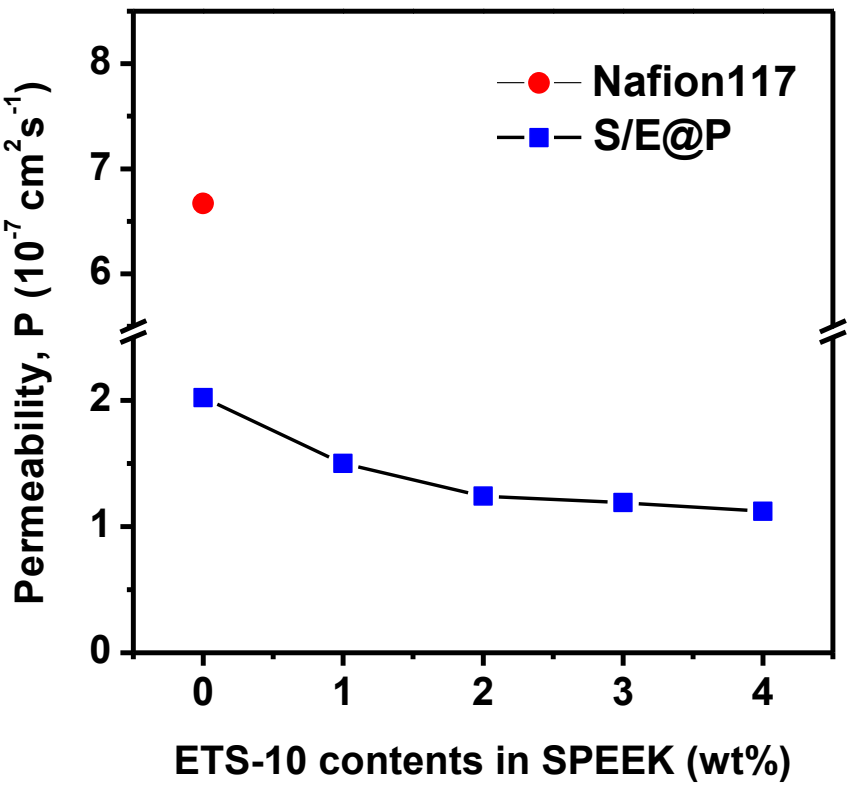


**Fig 30. Variation of vanadium permeability of N117 and S/E@P series membranes according to ETS-10 contents.**

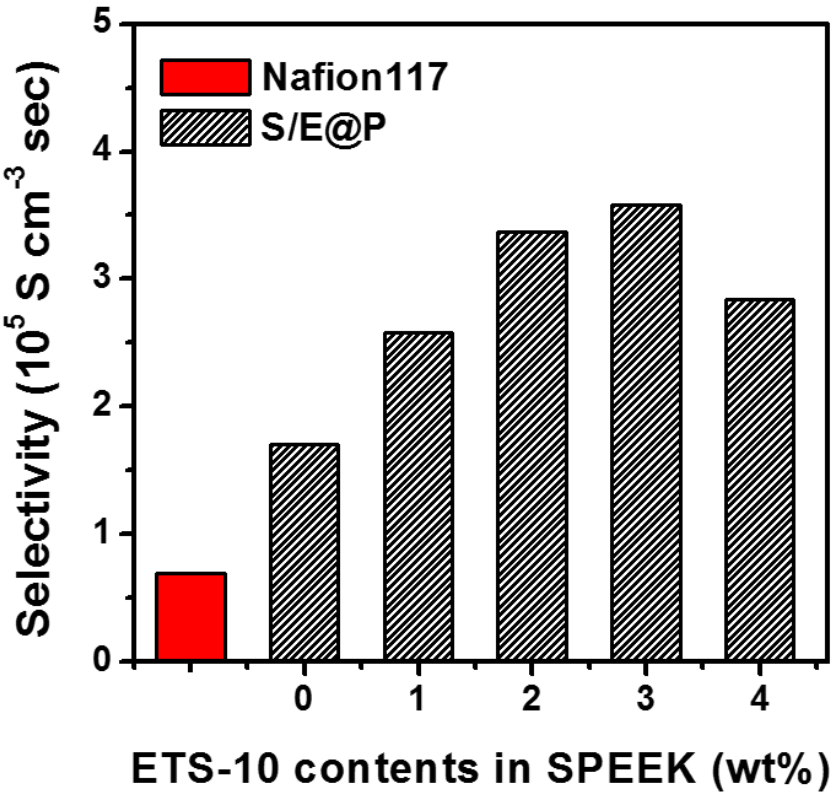


**Fig 31. Ion selectivity of N117 membrane and S/E@P series membrane.**

### 3.3.6. VRB single cell performance

The charge-discharge curves of VRBs with S/E@P membranes, and Nafion117 at the current density of 40, 60, 80, 100 mA $cm^{-2}$ are illustrated in Fig 32. The rank of charge and discharge capacity of membranes is S/E3@P > S/E2@P > S/E1@P > S/E4@P > N117 > S/E0@P at 80 mA $cm^{-2}$. The capacity of the membranes containing ETS-10 particles is larger than that of S/E0@P, indicating that the particle suppress the crossover of vanadium ion. Among the membranes, the S/E3@P membranes, which containing 3 wt% of ETS-10 particles, shows the largest capacity at all current densities. As mentioned in above selectivity results, this result can be explained by the good balance of proton conductivity and vanadium permeability of the membrane. S/E4@P membrane showed relatively large capacity at low current density. However, at high current density, the membrane showed low rank of capacity. This result can be explained that low vanadium ion permeability and large membrane resistance of S/E4@P membrane. At low current density, because charge-discharge time is relatively long, vanadium permeability is important to capacity than membrane resistance. On the other hand, at high current density, the

membrane resistance becomes important because larger amount of proton should pass the membrane at same time.

Fig 33 shows the result of the charge-discharge test with various pore-filled membrane at different current densities to confirm coulombic efficiency (CE), voltage efficiency (VE) and energy efficiency (EE).

The rank of CE is S/E4@P > S/E3@P > S/E2@P > S/E1@P > N117 > S/E0@P at 80 mA $cm^{-2}$, in accordance with the results on vanadium ion permeability. S/E0@P membrane shows lower CE than N117 membrane due to the low thickness of membrane. With the increasing of ETS-10 contents, the $VO^{2+}$ permeability of composite membranes decreases, leading to lower cross-mixing of vanadium ions and higher CE.

The VE is related with the efficiency of proton transport through membrane. The VE has an order of S/E3@P > S/E2@P > S/E1@P > S/E0@P > S/E4@P > N117 at 60 mA $cm^{-2}$. Although the N117 membrane shows the highest proton conductivity in above section, N117 shows the lowest VE at all current densities. It comes from the fact that the S/E@P membrane has the lower thickness (70 $\mu$m) than

N117 (210 $\mu$m). The proton pathway through Nafion117 is longer than that through S/E@P.

The EE indicate the energy conversion ability for large-scale VRB system. The rank of EE is S/E3@P > S/E2@P > S/E1@P > S/E0@P > S/E4@P > N117 at 80 mA $cm^{-2}$. The EE of S/E@P is higher than that of N117 membrane due to the better selectivity as discussed above. S/E3@P shows the best single cell efficiency of CE (99.1%), VE (81.6%) and EE (81.3%), while the Nafion117 shows the cell performance of CE (98.8%), VE (72%) and EE (71.2%) at 80 mA $cm^{-2}$. Overall, the remarkable improvement in cell efficiency can be mainly attributed to the performance of S/E@P pore-filled membranes in suppressing the cross-mixing of vanadium ions without proton conductivity loss.

To further investigate the stability of S/E@P pore-filled membranes in VRB under acidic and oxidizing conditions, the VRB assembled with all the aforementioned membranes were run for 100 cycles. The decline in discharge capacity is due to unbalanced transport of vanadium ions and water along with some side-reactions. The detailed cycle performance of the VRBs over 100 cycles at 40 mA $cm^{-2}$ is shown in Fig 34. N117, which shows high vanadium ion

permeability, shows 67.5% of capacity retention at the 100 cycle. However, the capacity retention of S/E0@P and S/E3@P membrane is 79.5%, 87.9% respectively. It can be due to the PTFE matrix which can suppress the swelling of membrane and improve the mechanical strength of membrane. The energy efficiency of various membranes are shown over 100 cycles. While the EE of N117 decline from 82% to 77%, S/E@P membranes are relatively constant over 80% of EE. The S/E3@P membrane shows higher EE than other S/E@P membranes, N117, pristine SPEEK, resulting from the low vanadium ion cross-mixing and higher conductivity. It can be conclude that S/E3@P pore-filled membrane possesses a superior chemical stability in vanadium solutions under acidic and oxidizing conditions.

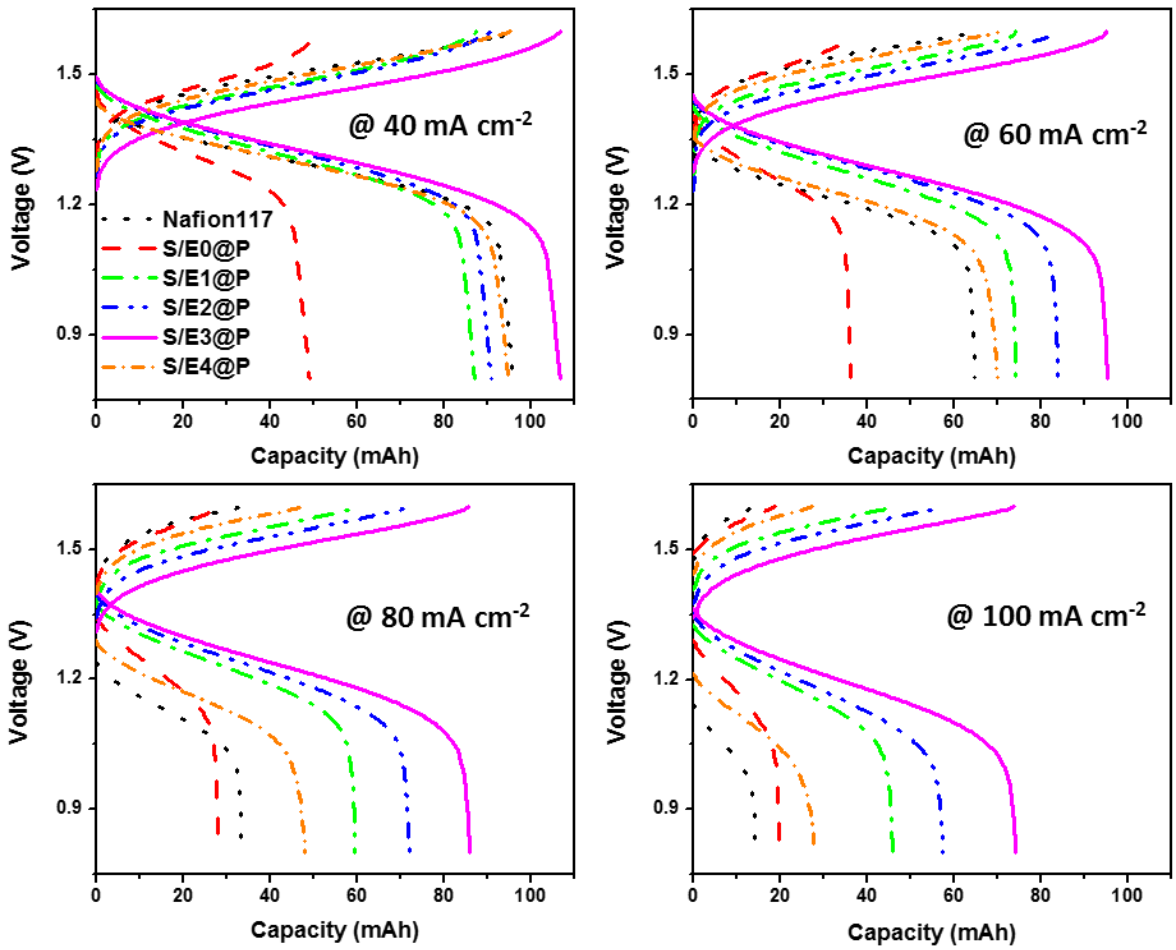


**Fig 32. Charge-discharge curves of VRBs with N117 and S/E@P series membranes at 40, 60, 80, 100 mA $cm^{-2}$.**

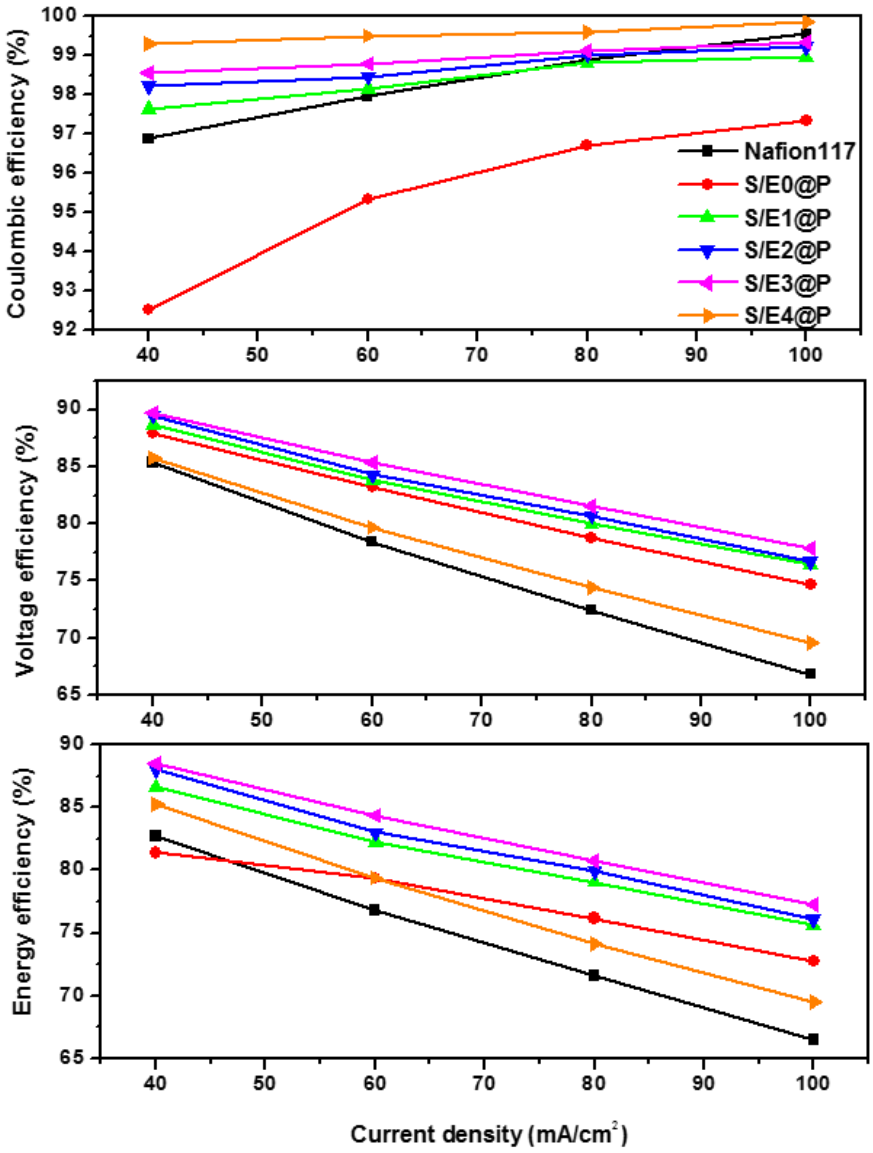


**Fig 33. Cell performance of VRBs with N117 and S/E@P series membranes under different current densities.**

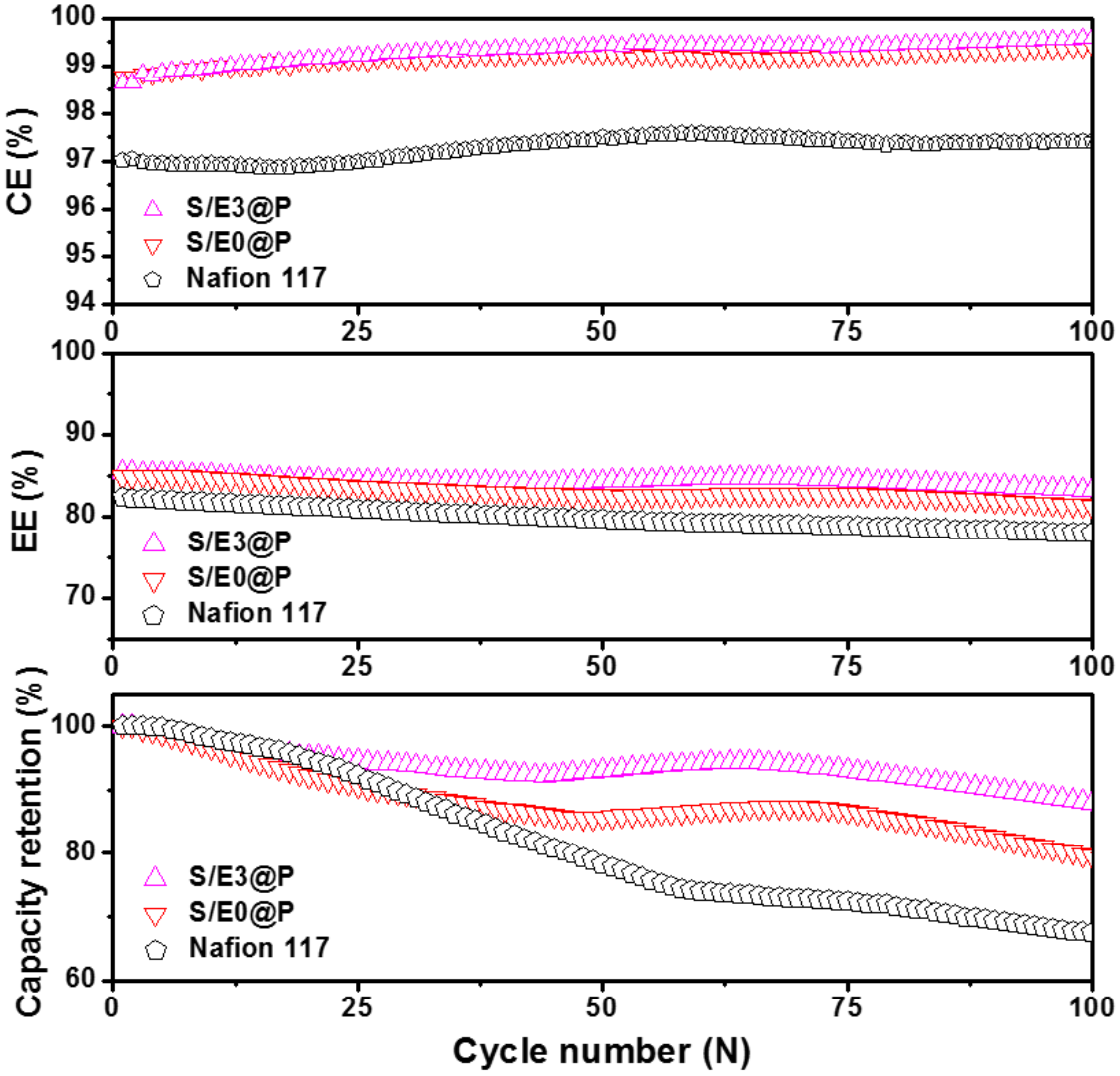


**Fig 34. Cycle performance of VRBs with N117, S/E0@P and S/E3@P membranes.**

## 4. Conclusions

In this study, ETS-10 particles are synthesized with various condition such as temperature, Ti source, Si source. The condition of 200 °C temperature, P25 Ti source, and colloidal silica Si source is the optimal for synthesis the ETS-10 with high crystallinity and particle size. To clarify the ETS-10 particle effect on VRBs membrane, the SPEEK/ETS-10 composite membranes are prepared by solution casting method with various ETS-10 contents. The cross-section morphology and EDS results of the membranes confirmed that ETS-10 particle uniformly dispersed over membranes and composite membranes are dense and homogeneous with no crack. The water uptake of the composite membranes increased gradually with increasing ETS-10 contents. This is due to the hydrophilicity of ETS-10. There is no proton conductivity loss up to 4 wt% ETS-10 loading and decreased upon further addition of ETS-10. The vanadium permeability of the composite membranes decreased with increasing ETS-10 contents resulting from blocking effect of inorganic particles. The single cell performance of VRBs assembled with the selected membranes was performed with various current density. The S/E4 membranes, which

contains 4 wt% ETS-10 in membrane matrix, showed the best VRB single cell performance of 99% CE, 80.0% VE and 79.2% EE at 80 mA $cm^{-2}$ due to its lower vanadium permeability without conductivity loss. In addition, the cycle performance of VRB assembled with composite membrane is relatively stable efficiency over 100 cycles compared to N117.

To further prolong the cycle stability of the SPEEK/ETS-10 composite membrane for long-life VRB applications, a PTFE-based pore-filling membranes was fabricated with various ETS-10 contents. To prevent the deposition of the ETS-10 particle in membrane, the contents of ETS-10 is limited up to 4 wt%. The SEM and EDS results of membranes confirmed that SPEEK polymer is successfully impregnated and the ETS-10 particles are dispersed homogeneously over PTFE matrix. The proton conductivity is increase as ETS-10 particle loading up to 3 wt% loading. The vanadium permeability of the pore-filled membrane decrease with increasing ETS-10 loading due to the blocking effect. The single cell performance of VRBs assembled with the pore-filled membranes was conducted with various current density from 40 to 100 mA $cm^{-2}$. S/E3@P showed the best efficiency of 99.1% CE, 81.6% VE, 81.3% EE at 80 mA $cm^{-2}$ among the membranes.

At cycle test, the VRBs with the S/E3@P membrane ran for up to 100 cycles with a very stable EE as well as relatively low capacity decline compared to N117 due to the fact that PTFE membrane suppress the swelling and improve the mechanical and chemical stability of the membranes. Overall, PTFE reinforced a SPEEK/ETS-10 composite membrane has great potential for usage in highly efficient and long-life VRB systems.

## 5. References


1. Dunn, B., H. Kamath, and J.-M. Tarascon, *Electrical energy storage for the grid: a battery of choices.* Science, 2011. **334**(6058): p. 928-935.

2. Chu, S. and A. Majumdar, *Opportunities and challenges for a sustainable energy future.* nature, 2012. **488**(7411): p. 294-303.

3. Wang, W., et al., *Recent progress in redox flow battery research and development.* Advanced Functional Materials, 2013. **23**(8): p. 970-986.

4. Rychcik, M. and M. Skyllas-Kazacos, *Characteristics of a new all-vanadium redox flow battery.* Journal of Power Sources, 1988. **22**(1): p. 59-67.

5. Ding, C., et al., *Vanadium flow battery for energy storage: prospects and challenges.* The Journal of Physical Chemistry Letters, 2013. **4**(8): p. 1281-1294.

6. Yang, Z., et al., *Electrochemical energy storage for green grid.* Chemical reviews, 2011. **111**(5): p. 3577-3613.

7. Skyllas-Kazacos, M., et al., *Progress in flow battery research and development.* Journal of the Electrochemical Society, 2011. **158**(8): p. R55-R79.

8. Prifti, H., et al., *Membranes for redox flow battery applications.* Membranes, 2012. **2**(2): p. 275-306.

9. Li, X., et al., *Ion exchange membranes for vanadium redox flow battery (VRB) applications*. Energy & Environmental Science, 2011. **4**(4): p. 1147-1160.

10. Dai, H., et al., *High performance composite membranes with enhanced dimensional stability for use in PEMFC.* international journal of hydrogen energy, 2010. **35**(9): p. 4209-4214.

11. Mohammadi, T. and M.S. Kazacos, *Evaluation of the chemical stability of some membranes in vanadium solution.* Journal of applied electrochemistry, 1997. **27**(2): p. 153-160.

12. Zhang, H., et al., *Nanofiltration (NF) membranes: the next generation separators for all vanadium redox flow batteries (VRBs)?* Energy & Environmental Science, 2011. **4**(5): p. 1676-1679.

13. Zeng, J., et al., *Studies on polypyrrole modified nafion membrane for vanadium redox flow battery.* Electrochemistry Communications, 2008. **10**(3): p. 372-375.

14. Teng, X., et al., *Nafion/organic silica modified TiO 2 composite membrane for vanadium redox flow battery via in situ sol–gel reactions.* Journal of Membrane Science, 2009. **341**(1): p. 149-154.

15. Dai, W., et al., *Sulfonated Poly (Ether Ether Ketone)/Graphene composite membrane for vanadium redox flow battery.* Electrochimica Acta, 2014. **132**: p. 200-207.

16. Winardi, S., et al., *Sulfonated poly (ether ether ketone)-based proton exchange membranes for vanadium redox battery applications.* Journal of Membrane Science, 2014. **450**: p. 313-322.

17. Mai, Z., et al., *Sulfonated poly (tetramethydiphenyl ether ether ketone) membranes for vanadium redox flow battery application.* Journal of Power Sources, 2011. **196**(1): p. 482-487.

18. Chen, D., et al., *Synthesis and properties of novel sulfonated poly (arylene ether sulfone) ionomers for vanadium*

*redox flow battery.* Energy Conversion and Management, 2010. **51**(12): p. 2816-2824.

19. Li, Y., et al., *Hydrophilic porous poly (sulfone) membranes modified by UV-initiated polymerization for vanadium flow battery application.* Journal of Membrane Science, 2014. **454**: p. 478-487.

20. Huang, R., et al., *Sulfonation of poly (ether ether ketone)(PEEK): kinetic study and characterization.* Journal of applied polymer science, 2001. **82**(11): p. 2651-2660.

21. Sambandam, S. and V. Ramani, *SPEEK/functionalized silica composite membranes for polymer electrolyte fuel cells.* Journal of power sources, 2007. **170**(2): p. 259-267.

22. Di Vona, M.L., et al., *SPEEK-TiO 2 nanocomposite hybrid proton conductive membranes via in situ mixed sol–gel process.* Journal of membrane science, 2007. **296**(1): p. 156-161.

23. Tricoli, V. and F. Nannetti, *Zeolite–Nafion composites as ion conducting membrane materials.* Electrochimica Acta, 2003. **48**(18): p. 2625-2633.

24. Yang, R., et al., *Colloidal silicalite-nafion composite ion exchange membrane for vanadium redox-flow battery.* Journal of Membrane Science, 2015. **484**: p. 1-9.

25. Kim, J., J.-D. Jeon, and S.-Y. Kwak, *Nafion-based composite membrane with a permselective layered silicate layer for vanadium redox flow battery.* Electrochemistry Communications, 2014. **38**: p. 68-70.

26. Jia, C., et al., *Sulfonated Poly (Ether Ether Ketone)/Functionalized Carbon Nanotube Composite Membrane for Vanadium Redox Flow Battery Applications.* Electrochimica Acta, 2015. **153**: p. 44-48.

27. Jeon, J.-D., J. Kim, and S.-Y. Kwak, *Nafion/microporous titanosilicate ETS-4 composite membranes for effective methanol crossover reduction in direct methanol fuel cells.* Journal of membrane Science, 2012. **415**: p. 353-359.

28. Changkhamchom, S. and A. Sirivat, *High proton conductivity ZSM-5/sulfonated poly (ether ketone ether sulfone)(S-PEKES) composite proton exchange membrane for using in direct methanol fuel cell.* Solid State Ionics, 2014. **263**: p. 161-166.

29. Sasikala, S., et al., *Functionalized Bentonite clay-sPEEK based composite membranes for direct methanol fuel cells*. Electrochimica Acta, 2014. **135**: p. 232-241.

30. Cui, Y., et al., *Enhancement of Nafion based membranes for direct methanol fuel cell applications through the inclusion of ammonium-X zeolite fillers.* Journal of Power Sources, 2015. **294**: p. 369-376.

31. Anderson, M., et al., *Microporous titanosilicate ETS-10: a structural survey.* Philosophical magazine B, 1995. **71**(5): p. 813-841.

32. Anderson, M., et al., *Structure of the microporous titanosilicate ETS-10.* Nature, 1994. **367**(6461): p. 347-351.

33. KerryáThomas, J., *Synthesis of microporous titanosilicates ETS-10 and ETS-4 using solid TiO 2 as the source of titanium.* Chemical Communications, 1996(12): p. 1435-1436.

34. Philippou, A., J. Rocha, and M.W. Anderson, *The strong basicity of the microporous titanosilicate ETS-10.* Catalysis letters, 1999. **57**(3): p. 151-153.

35. Wei, T.-C. and H.W. Hillhouse, *Ion transport in the microporous titanosilicate ETS-10.* The Journal of Physical Chemistry B, 2006. **110**(28): p. 13728-13733.

36. Teng, X., et al., *Ultra-thin polytetrafluoroethene/Nafion/silica composite membrane with high performance for vanadium redox flow battery.* Journal of Power Sources, 2014. **272**: p. 113-120.

37. Park, J.-S., et al., *An electrical impedance spectroscopic (EIS) study on transport characteristics of ion-exchange membrane systems.* Journal of colloid and interface science, 2006. **300**(2): p. 655-662.

38. Mihailova, B., et al., *Vibrational spectra of ETS-4 and ETS-10.* Zeolites, 1996. **16**(1): p. 22-24.

39. Eguizábal, A., et al., *Novel hybrid membranes based on polybenzimidazole and ETS-10 titanosilicate type material for high temperature proton exchange membrane fuel cells: A comprehensive study on dense and porous systems.* Journal of Power Sources, 2011. **196**(21): p. 8994-9007.

## 국문 초록


티타노 실리케이트 ETS-10 은 3 차원 구조의 미세기공을 지니고 있으며 구조적 특성에 의해 격자 내부에 -2 의 형식 전하를 가지는 물질이다. 최적의 기공 크기 및 특유의 기공 특성에 의하여 이온의 선택적인 투과 및 기공을 통한 프로톤의 전달에 용이하다.

본 연구에서는 바나듐 흐름전지에 사용되는 이온교환막의 첨가제로서 ETS-10 의 효과를 알아보기위해 술폰화 PEEK 에 ETS-10 을 입자함량을 달리하여 복합막을 제조하고 이 특성을 분석하였다. FE-SEM 및 EDS 분석을 통해 ETS-10 이 술폰화 PEEK 고분자 내부에 고르게 존재하는 것을 확인하였다. 함수율, 이온교환능, 기계적 특성, 프로톤 전도도 및 바나듐 투과도를 분석하였고 이를 바나듐 흐름전지의 이온교환막으로 사용하여 전지 성능 테스트를 실시하였다. 복합막의 프로톤 전도도는 4 wt%까지 입자 도입에 따라 술폰화 PEEK 와 비교하여 증가함을 확인하였다. 바나듐 투과도는 입자의 억제 효과에 의해 도입에 따라 감소하였다. 4 wt%의 입자가 도입된 복합막의 경우 샘플군 중 가장 높은 이온선택도를 보였으며, 셀 전지 성능평가에서 각각 99%의 쿨롱효율, 80.0%의 전압효율 및 79.2%의 에너지 효율을 보였다. 이는 전도도의 손실없이 바나듐 투과도가 증가한 결과로, 같은 조건에서 각각 98.8%의 쿨롱효율, 72.4%의 전압효율 및 71.4%의 에너지효율을

보인 상용막 Nafion117 보다 향상된 성능을 보였다. 게다가 장기성능평가에서 4wt%의 입자함량의 복합막이 높은 효율 및 용량보존율을 보였다. 이를 통해 ETS-10 입자가 전도도의 손실 없이 바나듐의 투과를 선택적으로 저감시킴으로써 전지 성능을 향상시키기에 적합한 첨가제임을 확인하였다.

다음으로, 바나듐 흐름전지의 장기성능안정성을 향상시키기 위해 PTFE 내에 SPEEK/ETS-10 의 복합막을 기공충진방식을 통해 제조하였다. 위와 동일한 분석 및 성능평가를 실시하였다. 기공충진 복합막의 경우 복합막에 비해 얇은 두께를 가졌다 (각각 70 μm 및 120 μm). 3 wt% 입자함량의 기공충진 막은 전지 성능 평가에서 각각 99.1%의 쿨롱효율, 81.9%의 전압효율 및 81.2%의 에너지 효율을 보였다. 이는 앞선 복합막 샘플군에 비해 높은 수치이다. 게다가 높은 수치안정성으로 인해 장기성능평가에서 Nafion117 보다 높은 효율 및 용량 보존율을 보였다. 이를 통해 PTFE 에 기공충진하는 방식을 통해 장기성능안정성이 향상됨을 확인하였다. 이를 통해 ETS-10 의 첨가 및 PTFE 를 통한 미세기공충진을 통해 제조된 막이 Nafion117 보다 높은 효율 및 장기성능안정성을 보임을 통해 이를 대체할 바나듐 흐름전지용 이온교환막으로 사용될 수 있는 가능성을 확인하였다.